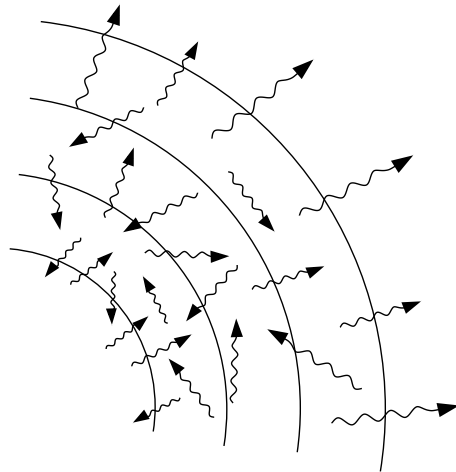# 3D Radiative Transfer in Radial Velocity Fields

University of Hamburg - Physics Department

Hamburger Sternwarte

Diploma Thesis

presented by

Lars Buntemeyer

September 21st, 2009

Universität Hamburg

hamburger sternwarte

Abstract

The modeling of stellar and planetary atmospheres is crucial for the understanding of astronomical observations. To understand how light that emerges from a stellar atmosphere is transported from the inner regions of origin to the outer layers we have to model radiative transfer and solve the radiative transfer equation (RTE). Earlier approaches of implementing the numerical solution of the RTE were restricted to one dimension (1D) and spherically symmetric atmospheres due to limited computational power.

Recent observations and theoretical calculations have shown the importance of non-spherically symmetric structures (e.g. supernovae). A solution of the three dimensional (3D) RTE then becomes essential for the modeling of realistic astronomical objects. Fortunately, increasing computational power of modern computers in the last years and parallel programming interfaces made it possible to fully implement solutions of the 3D-RTE.

In this work, we describe the theoretical background and a numerical solution of the 3D-RTE. Radial velocity fields are included in the model by considering special relativistic effects on the radiative transfer. This enables us to describe the dynamics of expanding or collapsing structures. We present a numerical solution scheme which has been implemented in the 3D radiative transfer framework of PHOENIX. The solver is based on a Gauss-Seidel iteration scheme and includes a formal solution based on the method of characteristics.

Finally, the implementation has been tested in line transition calculations of a simple two-level atom model. The results are compared to solutions of the 1D solver which is successfully implemented in the 1D radiative transfer framework of PHOENIX.

Zusammenfassung

Die Modellierung stellarer und planetarer Atmosphären ist entscheidend für unser Verständnis astronomischer Beobachtungen. Um zu verstehen, wie Licht aus den inneren Regionen eines Sterns in die äußere Atmosphäre transportiert wird, müssen wir die Theorie des Strahlungstransportes anwenden und die Strahlungstransportgleichung lösen. Frühere Ansätze zur numerischen Lösung des Strahlungstransportproblemes waren aufgrund mangelnder Rechnerleistungen und Speicherkapazität meist auf eindimensionale (1D) Lösungen beschränkt. Aktuelle Beobachtungen und theoretische Rechnungen zeigen allerdings, dass nicht sphärisch symmetrische Beschreibungen, wie z.B für Supernovae, immer wichtiger werden. Die Lösung der dreidimensionalen (3D) Strahlungstransportgleichung wird dabei ausschlagebend für unser Verständnis astronomischer Objekte. Glücklicherweise hat die Zunahme von Rechnerleistungen in den letzen Jahren und vor allem die Entwicklung paralleler Programmierschnittstellen uns die Möglichkeit eröffnet, die vollständige Lösung der 3D Strahlungstransportgleichung zu implementieren.

In dieser Arbeit beschreiben wir den theoretischen Hintergrund und eine numerische Lösung der 3D Strahlungstransportgleichung. Dabei werden radiale Geschwindigkeitsfelder in das Modell integriert, indem speziell-relativistische Effekte auf den Strahlungstransport betrachtet werden. Dies erlaubt es uns, die Dynamik expandierender oder kollabierender Strukturen zu beschreiben.

Unser numerisches Lösungsschema wurde in der 3D Strahlungstransportumgebung von PHOENIX implementiert. Der Lösungsansatz basiert auf einer Gauß-Seidel Iteration und beinhaltet eine formale Lösung, welche auf der Methode der Charakteristiken basiert.

Schließlich wurde die Implementation am Linienübergang eines hypothetischen 2-Niveau Atoms getestet. Die Ergebnisse wurden mit den Lösungen der 1D Strahlungstransportgleichung verglichen.

Contents

Chapter 1

Preface

The light of a star that reaches us and which an observer uses for spectroscopy leaves the stellar atmosphere in a relatively thin outer layer. In our sun, this layer is called the *photosphere*, and it is only about 500 km thick. This is the area where the athmosphere becomes optically thin, and light is able to leave the star whithout being scattered or absorbed. The theory of radiative transfer is crucial for the understanding of these processes. It enables us to describe the transport of energy from the inner regions, which we can not observe directly, to the outer layers of a stellar atmosphere. We can then create a model atmosphere which is crucial for the understanding of astronomical observations.

To verify a stellar model atmosphere, we have to compute synthetic spectra and compare them with the observed ones. This requires us to solve the radiative transfer equation (RTE). This can be a demanding challenge which depends on the complexity of the model astmosphere. To get realistic results, the RTE can become very complex because in order to describe an atmosphere accurately, we have to take in account numerous physical processes. For example, a photon which is travelling through an athmosphere, is scattered and absorbed due to numerous interaction processes between radiation and matter. In the outer optically thin regions, the photon can be scattered over long distances without being absorbed, and due to this, the energy sources of different regions in the atmosphere are coupled. This makes the solution of the RTE extremely complicated, because mathematically the RTE becomes an integro-differential equation. Due to that, we need efficient numerical tools in order to get a consistent solution of the RTE.

The simulation code used during the work on this thesis is part of the planetary and stellar atmosphere code, called `PHOENIX`, which has been developed by Prof. Peter H. Hauschildt (University of Hamburg) and Prof. Edward A. Baron (University of Oklahoma). `PHOENIX` can calculate atmospheres and spectra of stars and planets, including main sequence stars, giants, white dwarfs, stars with winds, TTauri stars, Novae, Supernovae, brown dwarfs and extrasolar giant planets [Hauschildt and Baron 1999]. The code is permanently extended and improved in order to get use of the advance in computational power of modern computers. The algorithms for the radiative transfer, spectral line opacity, NLTE opacity and rate calculations have been implemented for parallel computation [Hauschildt *et al.* 1997]. Parallel algorithms have become crucial since the radiative transfer calculations are extended to three dimensions (3D). The solution of the 3D-RTE has become a common research subject in computational astrophysics in the last years, as the deviation of the structures of all types of supernovae from spherical symmetry have been shown in [Wang and Wheeler 2008].

The intention of this thesis was to extend the `PHOENIX` code in order to describe the dynamics of a stellar atmosphere in 3D with radial velocity fields. The method we use to solve the 3D-RTE is

based on the method described by Mihalas for solving the special relativistic spherically symmetric RTE (SSRTE) [Mihalas 1980]. We extend the method, since we want to solve the full 3D-RTE for non-spherically symmetric atmospheres in general.

At first, we describe the basics of the theory of radiative transfer in chapter 2, where we concentrate mostly on the derivation of the special relativistic RTE. In Chapter 3, we describe Mihalas' method for the numerical solution of the SSRTE, and how we adapted it for the implementation in the 3D transfer framework of PHOENIX. We summarize computational aspects that are crucial for numerical 3D radiative transfer and discuss the results of our test calculations in chapter 4. Finally, we give an outlook on actual and future research subjects in the theory of radiative transfer in chapter 5.

Chapter 2

The Theory of Radiative Transfer

The goal of the theory of radiative transfer in astrophysics is to describe the energy flow through the different layers of a stellar or planetary atmosphere. We have to apply known physical laws about absorption and scattering processes and derive the characteristic observables from the theory. We then compare the theoretical results with observations and can improve our model. In this chapter we describe the basic theory of radiative transfer. We introduce the important physical values which we need to describe the transfer of energy through the atmosphere. We describe the crucial scattering problem which makes the solution of the radiative transfer equation (RTE) a demanding numerical problem. At the end of the chapter, we introduce special relativistic radiative transfer and present the spherical symmetric special relativistic radiative transfer equation (SSRTE). If not explicitly referenced otherwise, the contents of this chapter are based on [Mihalas 1978].

2.1   How We Measure Radiative Transfer

The radiation field consists of photons with energies defined by their momenta $p = h\nu/c$. If we know the energy and direction of propagation $\vec{n}$ of each photon in the radiation field, we can describe it by a *photon distribution function* $f(\vec{x}, \vec{p}, t)$ which is defined as in [Gray 1992] by

$$dN(\nu) = f(\vec{x}, \vec{p}, t) \, d\vec{p} \, dV \tag{2.1}$$

with the fequency ν. The radiation field is then described as a photon gas with the phase space density f. However, this is a microscopic description and not common in the formulation of radiative transfer, since we are not interested in the observation of single photons. The spectrum, an observer detects, measures the dependency of the overall energy transported by photons in a specific frequency interval $(\nu, \nu + d\nu)$ on the frequency. Thus, we use an energy description of the radiation field which is equivalent to (2.1) by defining the *specific intensity I* being proportional to f via

$$f(\vec{x}, \vec{p}, t) \, d\vec{p} = \frac{dN(\nu)}{dV} = \frac{1}{h\nu c} \, I(\vec{x}, \vec{n}, \nu, t) \, . \tag{2.2}$$

The specific intensity describes the intensity of radiation at position $\vec{x}$ and frequency ν traveling in direction $\vec{n}$ at time t so that the energy dE which is transported through the unit area dA in $\vec{x}$ into the solid angle $d\omega$ by radiation of frequencies $(\nu, \nu + d\nu)$ in the time interval $(t, t + dt)$ is defined as

$$dE = I(\vec{x}, \vec{n}, \nu, t) \, dA \, \cos\theta \, d\omega \, d\nu \, dt \tag{2.3}$$
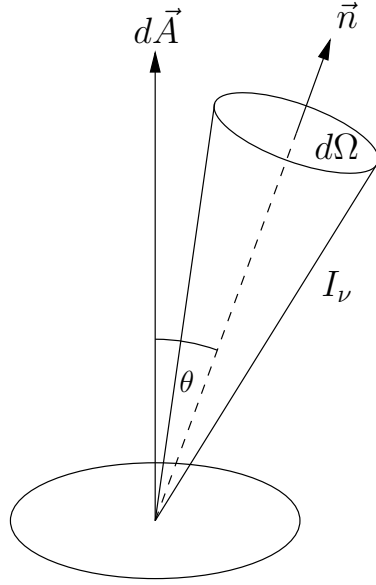
Figure 2.1: The geometrical situation for the definition of the specific intensity I. The vector $d\vec{A}$ is perpendicular to the unit area dA and $\vec{n}$ describes the direction of propagation of the specific intensity.

Here, θ is the angle between the direction of propagation of I and the normal to the surface $(dA\cos\theta = \vec{n} \cdot d\vec{A})$. In the following, we will often use the angle cosine μ defined as $\mu = \cos\theta$. In addition, we will often refer to the importance of the frequency dependency and for better readibility, we will write ν as a subscript from now on.

The average of I_ν over all solid angles is called the *mean intensity*

$$J_\nu(\vec{x}, t) = \frac{1}{4\pi} \int_{4\pi} I_\nu(\vec{x}, \vec{n}, t) \, d\Omega \tag{2.4}$$

We describe the direction of propagation $\vec{n}$ in spherical coordinates (θ, ϕ). With $d\Omega = \sin\theta d\theta d\phi = -d\mu d\phi$ and $\mu = cos\theta$ we can rewite J as

$$J_\nu(\vec{x}, t) = \frac{1}{4\pi} \int_0^{2\pi} \int_{-1}^1 I_\nu(\vec{x}, \mu, \phi, t) \, d\mu \, d\phi$$

The mean intensity is an angular average of the specific intensity. It is useful for statistical processes, where the origin of the photons is not of interest (like radiative excitation and ionization).

The *monochromatic flux* is the net flow of energy per second through an area at $\vec{x}$ perpendicular to $\vec{n}$. In general, flux is a vector and can be defined by its components

$$\vec{F}_\nu(\vec{x}, t) = (\oint I_\nu(\vec{x}, \vec{n}, t) \, p_x \, d\Omega, \oint I_\nu(\vec{x}, \vec{n}, t) \, p_y \, d\Omega, \oint I_\nu(\vec{x}, \phi, \theta, t) \, p_z \, d\Omega)$$

where $\vec{p} = (p_x, p_y, p_z)$ denotes the direction of the flux in Cartesian coordinates. In fact, we often imply the radial direction for the flux so that we can write the radial flux in spherical coordinates

$$F_\nu^r(\vec{x}, \vec{n}, t) = \oint_{4\pi} \mu \, I_\nu(\vec{x}, \vec{n}, t) \, d\Omega$$

$$= \int_0^{2\pi} \int_{-1}^1 \mu \, I_\nu(\vec{x}, \mu, \phi, t) \, d\mu \, d\phi \tag{2.5}$$

The flux is a directional quantity for measuring radiative transfer through stellar and planetary atmospheres. In the case of thermodynamic equilibrium in the atmospheric layers, the net flux vanishes.

2.2 The Interaction of Radiation with Matter

As radiation is transported through an atmosphere, it is constantly interacting with the present matter. During these processes, energy is exchanged between the radiation field and the thermal energy of the atmosphere, also referred to as the *thermal pool* of the atmosphere. It is important to distinguish the interaction processes, because they have different effects on how energy is exchanged locally and globally between radiation and matter.

If we consider a beam of photons travelling through an atmosphere in a certain direction, energy can be removed or added to the beam during the interaction processes. Although in fact, the interaction processes are numerous, we distinguish between two basic ones. This allows us to introduce macroscopic coefficients in order to include the interaction processes into our model.

If energy is added to the beam, we call it an *emission process*. If energy is removed from the beam, we call it an *absorption process*. During an absorption process, a photon from the beam is destroyed, and its energy is converted partly or wholly into kinetic energy of particles in the atmosphere. In the other way, kinetic energy of a particle from the atmosphere is converted into a photon during an emission process. By this, thermal absorption and emission processes cause a direct energy exchange of the radiation field with the thermal energy of the gas in the atmosphere. If the mean free path of a photon in the atmosphere is much smaller than the distance on which the temperature considerably changes, the thermodynamic properties of the gas can be assumed to be in a *local thermodynamic equilibrium* (LTE). In this case, thermal absorption and emission couples the radiation field to the thermal pool at the region of interaction. The thermal absorption and emissions rates are then determined by the local thermodynamic properties of the gas.

Though the thermal absorption and emission processes itself are manifold, we want to distinguish the following three

a) *bound-free absorption and emission (b-f)*
   In fact, b-f absorption is simply *photoionization*. The energy of a photon is used to ionize an atom. Energy from the radiation field is converted into kinetic energy of an electron in the electron gas. The inverse emission process is the radiative recombination of an ion with a free electron. The b-f processes transfer energy back and forth between the radiation field and the thermal pool of the gas.

b) *free-free absorption and emission (f-f)*
   When a free electron of the electron gas is moving in the field of an ion, its kinetic energy can be changed by the absorption of a photon. The inverse process is called *bremsstrahlung* and emits an electron into the radiation field.

c) *bound-bound absorption (b-b)*
   b-b absorption is also known as *photoexcitation*. An electron that is bound in the field of an atom can be shifted to a higher bound level by the absorption of a photon. The excited atom can then be deexcited by an inelastic collision in the gas. By this, the energy of the photon is converted into thermal energy of the gas.

The deexcitation of an atom that is excited by photoexcitation (b-b absorption) can also happen by the immediate return of the bound electron into its ground state. The energy of the re-emitted photon is then only slightly shifted, and there is only little exchange of energy between the radiation field and the gas. But in general, the direction of propagation of the photon has changed. If a photon is removed from a beam of radiation by only changing its direction, we call this a *scattering process*. Though the energy of the photon is not converted into thermal energy of the gas during a scattering process, the change of the propagation direction causes an effective contribution to the absorption rate of the direction the photon is removed from. As a scattering process does not really destroy the photon, the pure thermal absorption is sometimes also called *true* absorption. The scattered photon however is added to a beam of a different direction. By this, a scattering process also causes an additional contribution to the total emission rate of the direction the photon is added to.

The crucial point with scattering processes is that the energy of the photon is not converted into thermal energy of the region where the scattering process takes place. If a scattered photon is able to travel over long distances, on which the change in temperature becomes important, the LTE assumption is no longer valid. In this non-LTE (NLTE) situation, energy of the radiation field can be transported over long distances in the atmosphere without an exchange with the local thermal pool. This causes a decoupling of the radiation field from the gas and its local thermodynamic properties. On the other hand, scattering processes can couple different regions of the atmosphere, when a scattered photon that originates in a different region is truly absorbed in another, and thus causes a contribution to the local thermal energy of the region of absorption. This situation is known as the *scattering problem*, because it makes the solution of the radiative transfer equation very demanding.

2.2.1   The Extinction Coefficient

The sum of all true and scattering absorption contributions is described by the *total absorption coefficient*, also called *extinction coefficient* or *opacity*. We define the *extinction coefficient* $\chi_\nu(\vec{x}, \vec{n}, t)$ by the energy removed from the beam

$$dE^- = \chi_\nu(\vec{x}, \vec{n}, t)\, I_\nu(\vec{x}, \vec{n}, t)\, dA\, \cos\theta\, ds\, d\omega\, d\nu\, dt \tag{2.6}$$

As described in the last section, extinction consists of thermal absorption and scattering processes. So we divide the extinction coefficient into

$$\chi_\nu(\vec{x}, \vec{n}, t) = \kappa_\nu(\vec{x}, \vec{n}, t) + \sigma_\nu(\vec{x}, \vec{n}, t) \tag{2.7}$$

where κ_ν is the thermal or true absorption contribution and σ_ν is the scattering coefficient. The dimension of χ_ν is $\frac{1}{\text{length}}$.

χ_ν includes also the stimulated emission caused by photons of the beam. These photons can perturb excited electrons in their bound-states causing the emission of another photon. Because the perturbing and the emitted photon are correlated in their direction of propagation, stimulated emission can cancel out some of the total opacity. Therefore, χ_ν will include the stimulated emission as a contribution of negative opacity.

In fact, the interaction of the radiation field and the absorbing matter of the atmosphere is not linear, because the radiation field is determined by the absorption rates, and the absorption rates themselves are determined by the level populations of the matter. On the other hand, the level populations are determined by the radiation field, because of stimulated and thermal emission

and absorption. Anyway, we can calculate the level populations in quantum theory in the case of LTE. For that, we have to solve the rate equations. In LTE, this problem simplifies to solving the Boltzmann- and Saha-equations which describe the level populations of bound and continuum states. The level populations can then be derived from the local density and temperature. But in the NLTE situation, the temperature itself is determined by the *global* balance between energy emitted and absorbed by the matter. Therefore, the temperature structure of the atmosphere depends also on the radiation field and its response to the global properties of the atmosphere. It is crucial to include the NLTE situation into a model atmosphere, because otherwise, we will get no realistic results.

2.2.2   The Emission Coefficient

The emission coefficient, also called *emissivity*, is defined by the energy added to a beam along the infinitesimal line element ds

$$dE^+ = \eta_\nu(\vec{x}, \vec{n}, t) \; dA \; \cos\theta \; ds \; d\omega \; d\nu \; dt$$

As described in the beginning of this section, we can also divide the emissivity into a thermal and scattering part

$$\eta_\nu(\vec{x}, \vec{n}, t) = \eta_\nu^\sigma(\vec{x}, \vec{n}, t) + \eta_\nu^\kappa(\vec{x}, \vec{n}, t)$$

Because of the statistical nature of absorption, scattering and emission processes, the opacity and emissivity are isotropic. But this is only true in a static atmosphere. In the presence of a velocity field, the opacity and emissivity become angle-dependent. However, we will drop the explicit angle-dependency for now, because we will solve the transfer equation in a comoving frame, where extinction and emission coefficients remain isotropic.

The thermal part of the emissivity $\eta_\nu^\kappa(\vec{x}, t)$ at the position $\vec{x}$ in the atmosphere depends on the local temperature $T(\vec{x})$ of the gas. We assume a thermodynamic equilibrium at $\vec{x}$, and in this case, thermal absorption and emission will be balanced. The thermal emission can be described by a Planck-emission and thus, the thermal absorption coefficient becomes

$$\eta_\nu^\kappa(\vec{x}, t) = \kappa_\nu(\vec{x}, t) \; B_\nu(T(\vec{x}), t)$$

This is known as the *Kirchhoff-Planck relation*. In the case of LTE, we can rewrite the emissivity as

$$\eta_\nu(\vec{x}, \vec{n}, t) = \eta_\nu^\kappa(\vec{x}, \vec{n}, t)$$

Again, because the overall radiation field itself determines the local thermal properties of the gas and vice versa, this simplifications becomes invalid in a realistic atmosphere. Hence, we have to include the scattering part η_ν^σ.

As mentioned before, the scattering part describes the global influence of the radiation field on local thermodynamic properties. That means, we have to take in account the contribution of scattered photons from all over the atmosphere in order to calculate the emission at a specific point $\vec{x}$ in the atmosphere. Though we do not know these contributions in the case of NLTE, we can write it formally as a scattered contribution from the incoming intensities from all directions at $\vec{x}$. Because we defined the mean intensity in (2.4), we can write the scattering contribution as

$$\eta_\nu^\sigma(\vec{x}, t) = \sigma_\nu(\vec{x}, t) \; J_\nu(\vec{x}, t)$$

With this, we can rewrite the emissivity as

$$\eta_\nu(\vec{x}, t) = \sigma_\nu(\vec{x}, t) \; J_\nu(\vec{x}, t) + \kappa_\nu(\vec{x}, t) \; B_\nu(T(\vec{x}), t) \tag{2.8}$$

2.2.3   The Source Function

A useful quantity, we will often use, is the ratio of emission and extinction. This is called the *source function* and it is defined as

$$S_\nu = \frac{\eta_\nu}{\chi_\nu} \tag{2.9}$$

The source function measures whether energy is removed or added to the radiation field. In the case of coherent scattering, we can use (2.8) and (2.7) to rewrite the monochromatic source function

$$S_\nu = \frac{\sigma_\nu}{\kappa_\nu + \sigma_\nu}\, J_\nu + \frac{\kappa_\nu}{\kappa_\nu + \sigma_\nu}\, B_\nu$$

and with the definition of the *thermal coupling parameter* ϵ we get

$$S_\nu = (1 - \epsilon)J_\nu + \epsilon B_\nu \tag{2.10}$$

$$\epsilon = \frac{\kappa_\nu}{\kappa_\nu + \sigma_\nu} \tag{2.11}$$

The thermal coupling parameter ϵ is the probability for the complete destruction of a photon during a thermal absorption process. Therefore, $\epsilon = 1$ means that all photons are thermalized and we do not have any scattering processes. In this case we get

$$S_\nu = B_\nu \tag{2.12}$$

which means that the radiation field is determined by pure thermal black-body radiation. This situation is equivalent to LTE.

2.3   The Radiative Transfer Equation

With the definitions of the specific intensity (2.3), the extinction coefficient (2.7), the emissivity (2.8), and the source function (2.9), we can now derive the radiative transfer equation. Figure (2.2) shows the geometrical situation, in which the incoming intensity $I_\nu(\vec{x})$ is partially reduced while passing through a disk of matter of area dA and thickness ds. At the same time, energy is emitted inside the disk and added to the outgoing intensity $I_\nu(\vec{x} + d\vec{x})$.
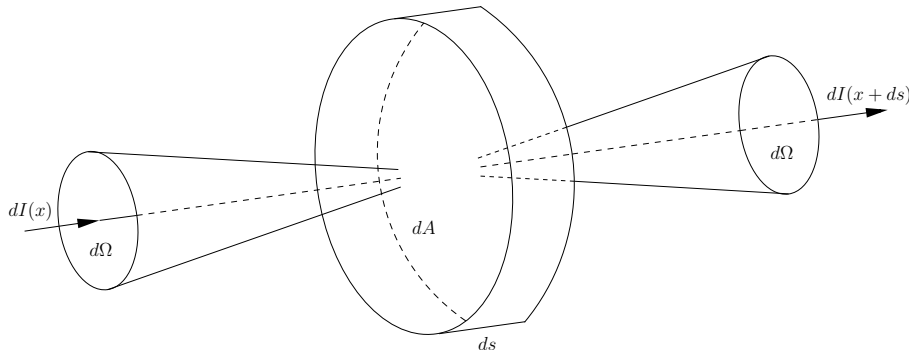

Figure 2.2: The incoming intensity is partly extinct inside the infinitesimal disk of matter. The outgoing intensity is the sum of the remaining incoming intensity and the emitted energy from inside the disk.

The difference between the incoming and outgoing intensities must be determined by the difference between the emitted and extinct energy inside the disk

$$[I_\nu(\vec{x} + \Delta\vec{x}, \vec{n}, t+\Delta t) - I_\nu(\vec{x}, \vec{n}, t)]\, dA\, d\omega\, d\nu\, dt$$

$$= [\eta_\nu(\vec{x}, \vec{n}, t) - \chi_\nu(\vec{x}, \vec{n}, t)I_\nu(\vec{x}, \vec{n}, t)]\, ds\, dA\, d\omega\, d\nu\, dt \;. \tag{2.13}$$

In the case of an infinitesimal disk, the difference between the intensities becomes a differential

$$dI_\nu(\vec{x}, t) = \left(\frac{\partial I_\nu}{\partial t}\right) dt + \left(\frac{\partial I_\nu}{\partial s}\right) ds$$

and with $dt = \frac{ds}{c}$

$$dI_\nu(\vec{x}, t) = \left[\frac{1}{c}\left(\frac{\partial I_\nu}{\partial t}\right) + \left(\frac{\partial I_\nu}{\partial s}\right)\right] ds \tag{2.14}$$

From the combination of (2.13) and (2.14), we get the time-dependent radiative transfer equation

$$\left[\frac{1}{c}\frac{\partial}{\partial t} + \frac{\partial}{\partial s}\right] I_\nu(\vec{x}, \vec{n}, t) = \eta_\nu(\vec{x}, \vec{n}, t) - \chi_\nu(\vec{x}, \vec{n}, t)I_\nu(\vec{x}, \vec{n}, t) \tag{2.15}$$

The differentiation $\frac{\partial}{\partial s}$ depends on the coordinate system in which I_ν is described. In a Cartesian coordinate system, we can derive

$$\frac{\partial}{\partial s} = \vec{n} \cdot \vec{\nabla} \tag{2.16}$$

In the case of time-independence, equation (2.15) becomes

$$\frac{\partial I_\nu(\vec{x}, \vec{n})}{\partial s} = \eta_\nu(\vec{x}, \vec{n}) - \chi_\nu(\vec{x}, \vec{n})I_\nu(\vec{x}, \vec{n}) \tag{2.17}$$

The RTE can be simplified by using the *optical depth* τ which is defined by its differential

$$d\tau_\nu(\vec{x}) = -\chi_\nu(\vec{x})\, ds \tag{2.18}$$

We define it with a negative sign so that the optical depth is zero at the surface of the atmosphere and increases inwards. Hence to get the optical depth that prevents a photon deep inside the atmosphere at radius r from leaving the star, we have to integrate τ from the surface at r_0 to r. We get the total radial optical depth from

$$\tau_\nu(r) = -\int_{r_0}^{r} \chi_\nu(r')\, dr' = \int_{r}^{r_0} \chi_\nu(r')\, dr'$$

With the definition of the optical depth (2.18) and the source function (2.9), we can write the general time-independent RTE in a very compact form by dividing it by the extinction coefficient χ_ν

$$\frac{\partial I_\nu}{\partial \tau_\nu} = I_\nu - S_\nu \tag{2.19}$$

Though it looks very compact and simple, the left hand side of (2.19) depends on the actual geometry of our transfer problem. Thus it can become very complex. Furthermore, when we

insert the source function from (2.10) which contains the mean intensity as defined in (2.4), equation (2.19) becomes

$$\frac{\partial I_\nu}{\partial \tau_\nu} = I_\nu - \left[(1-\epsilon) \left(\frac{1}{4\pi} \oint_{4\pi} I_\nu \, d\Omega \right) + \epsilon B_\nu \right] \tag{2.20}$$

Here we recognize that the RTE contains what we called the scattering problem. The differential equation for I_ν contains the integral over I_ν. This makes the RTE an *integro-differential equation*. Physically, this describes the decoupling of the radiation field from local thermodynamic properties in the case of NLTE. It means that for the solution of the RTE at a specific point in the atmosphere, we already have to know its solution everywhere else. To solve the RTE, we have to find consistent solutions of the source function S_ν and the radiation field described by I_ν and J_ν which satisfy (2.20).

2.3.1   The Formal Solution

Though the RTE (2.19) is an integro-differential equation, we can derive a *formal solution*. We can make (2.17) an exact differential equation by multiplying it with the factor $e^{-\chi s}$. The RTE (2.17) then becomes

$$\left[\chi_\nu I_\nu e^{-\chi_\nu s} + \eta_\nu e^{-\chi_\nu s} \right] ds + e^{-\chi_\nu s} dI_\nu = 0$$

We can then integrate the term in brackets from s_1 to s_2 and with our definition of the optical depth (2.18), we find the formal solution

$$I_\nu(\tau_2) = I_\nu(\tau_1) \, e^{(\tau_1 - \tau_2)} + \int_{\tau_1}^{\tau_2} S_\nu(\tau) \, e^{(\tau - \tau_2)} d\tau \tag{2.21}$$

The formal solution describes, what we see in figure (2.2). The first summand describes the incoming intensity which is damped exponentially along the direction of propagation from τ_1 to τ_2 due to extinction. The integral describes the intensity added to the beam between τ_1 and τ_2. At the same time, the emitted energy is also damped because of extinction. We call this a formal solution, because in general, we still do not know the source function in the integrand. However, the formal solution will become very important during the numerical solution described in chapter 3.

2.3.2   The Radiative Transfer Equation in 3D Spherical Coordinates

In this thesis, we want to describe radiative transfer in 3D spherical coordinates. These are the most accurate coordinates to describe the physical properties of a spherical shaped atmosphere. In a spherical coordinate system, the spatial point $\vec{x}$ is describes by three coordinates

$$\vec{x} = \vec{x}(r, \Theta, \Phi)$$

For the propagation vector of the specific intensity $\vec{n}$, we need another set of spherical coordinates (r', θ, ϕ). Because we are only interested in the direction of these coordinates, we can write

$$\vec{n} = \vec{n}(\theta, \phi)$$

Now we can write the specific intensity $I_\nu(\vec{x}, \vec{n})$ at the point $\vec{x}(r, \Theta, \Phi)$ in the spherical coordinates as

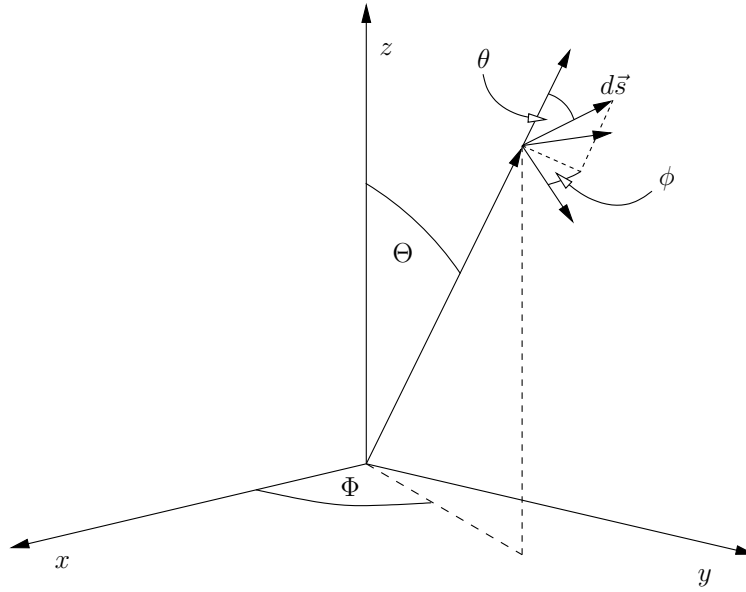$$I_\nu(r, \Theta, \Phi, \theta, \phi)$$

Figure 2.3: The global coordinate system which describes the atmosphere, and a local tangential coordinate
system in which we describe the direction of propagation;

It is important to keep in mind the difference between the local coordinates of propagation (θ, ϕ) and the point $x(r, \Theta, \Phi)$ in the global coordinate system, which describes the physics of an atmosphere.

To describe radiative transfer in 3D spherical coordinates, we have to write down explicitly the directional derivative on the left hand side of the time-independent RTE (2.17)

$$\frac{\partial}{\partial s} = \sum_{i=1}^{n} \frac{\partial x_i}{\partial s} \frac{\partial}{\partial x_i} \tag{2.22}$$

$$= \left(\frac{\partial r}{\partial s}\right)\left(\frac{\partial}{\partial r}\right) + \left(\frac{\partial \Theta}{\partial s}\right)\left(\frac{\partial}{\partial \Theta}\right) + \left(\frac{\partial \Phi}{\partial s}\right)\left(\frac{\partial}{\partial \Phi}\right) +$$
$$\left(\frac{\partial \theta}{\partial s}\right)\left(\frac{\partial}{\partial \theta}\right) + \left(\frac{\partial \phi}{\partial s}\right)\left(\frac{\partial}{\partial \phi}\right) \tag{2.23}$$

The derivatives with respect to θ and ϕ account for the change of the local tangential coordinate system. The spatial derivatives $\frac{\partial r}{\partial s}$, $\frac{\partial \Theta}{\partial s}$, and $\frac{\partial \Phi}{\partial s}$ describe the dependency of I_ν on the 3D coordinate system of the atmosphere. However, the 3D coordinates (r, Θ, Φ) depend on the direction of propagation $\vec{n}(\theta, \phi)$, since a photon in an inertial system always travels along a straight line of sight. Therefore, a fixed direction $\vec{n}$ determines the 3D coordinates (r, Θ, Φ) along which the specific intensity I_ν propagates. This implies that we can solve the 3D-RTE by solving a spherically symmetric RTE along several *characteristics* (section 3.3). We can drop the explicit dependencies of Θ and Φ in the RTE and use the spherically symmetric RTE if we solve it for all initial values of the direction of propagation $\vec{n}$. Thus, we will derive the spherically symmetric RTE in the following.

The derivative of the azimuthal angle ϕ vanishes in the case of spherically symmetric radiative transfer due to the rotational symmetry of a tangential frame in a spherically symmetric atmo-
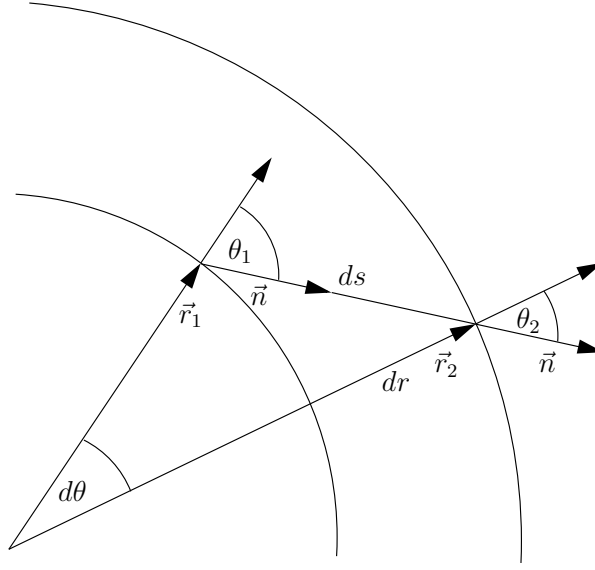
Figure 2.4: the parallel translation of $\vec{n}$ along $d\vec{s}$; in the case of spherical symmetry, the derivative with respect to ϕ vanishes.

sphere. Figure 2.4 shows the geometrical situation of an infinitesimal translation along $\vec{n}$. The derivatives with respect to r and the polar angle θ can be derived from the definitions of the trigonometric functions

$$\frac{\partial r}{\partial s} = \cos\theta \tag{2.24}$$

$$\frac{\partial \theta}{\partial s} = -\frac{\sin\theta}{r} \tag{2.25}$$

With (2.24) and (2.25), the directional derivative in the case of spherical symmetry becomes

$$\frac{\partial}{\partial s} = \mu\frac{\partial}{\partial r} + \frac{(1-\mu^2)}{r}\frac{\partial}{\partial \mu}$$

with $\mu = \cos\theta$.

We can now write down the spherically symmetric RTE

$$\left[\frac{1}{c}\frac{\partial}{\partial t} + \mu\frac{\partial}{\partial r} + \frac{(1-\mu^2)}{r}\frac{\partial}{\partial \mu}\right]I_\nu = \eta_\nu - \chi_\nu I_\nu \tag{2.26}$$

2.4 Radiative Transfer in Moving Media

The intention of this thesis is to solve the 3D-RTE for a dynamic atmosphere in the presence of a velocity field. But at this point, we only have an accurate description of radiative transfer for static media. To include a velocity field into our model, we have two choices for the description of the radiative transfer.

On the one hand, we can describe the transfer problem in the frame, where the observer at infinity and the center of the star are at rest. We call this frame the observer's frame or *Eulerian frame*.

But due to Doppler-shifts which we observe in an Eulerian frame with a velocity field, the Eulerian approach gets inconvenient when we want to compute spectral lines. To compute a synthetic spectrum, we have to include atomic and molecular data which we get from precomputed data bases. The line profiles are dynamically discretized for the computations in numerical radiative transfer. Figure 2.5 shows how the Doppler-shifts in an Eulerian frame will then make the discretization inaccurate. The wavelengths are shifted but the discretization grid is static.
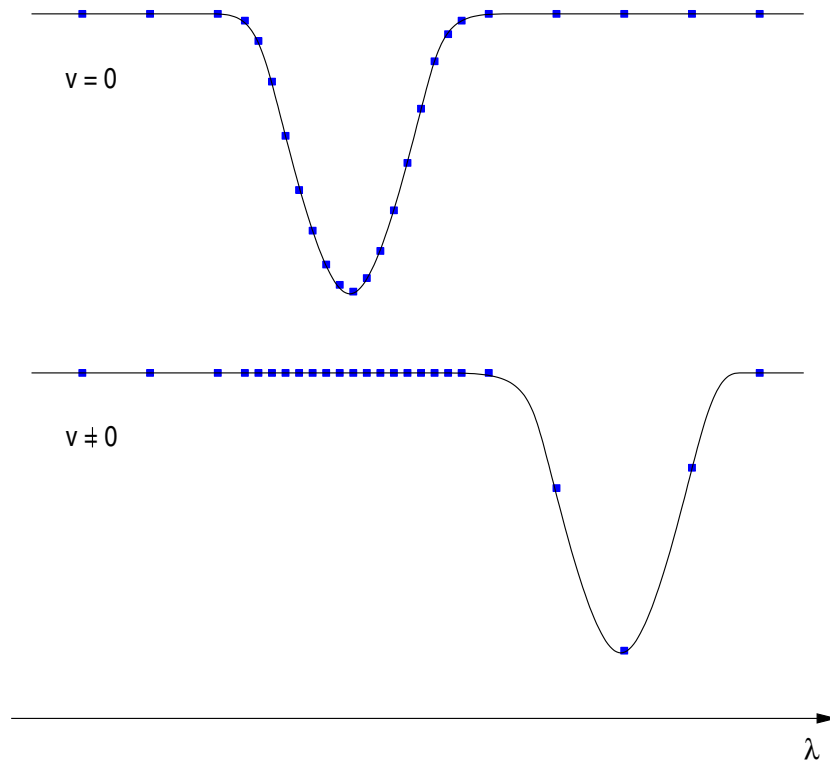

Figure 2.5: The dynamic wavelength sampling of a line in an Eulerian frame will not be accurate with velocity fields because of Doppler shifts in the line profile.

Furthermore, the Eulerian frame frequency depends on the angle between the direction of propagation $\vec{n}$ and the velocity $\vec{v}$ (see 2.32). Hence the opacity and emissivity also become angle-dependent, because they depend on the frequency. Therefore, the opacities and emissivities are not isotropic in the Eulerian frame.

On the other hand, we can describe the radiative transfer in a frame which is comoving with the atmosphere [Mihalas 1980]. We call this a *Lagrangian frame*. Because in a *comoving frame* (cmf) the velocity vanishes, there are no Doppler-shifts in the line profiles and the discretization stays accurate. We can then restrict the frequency-bandwidth, in which the line profile has to be discretized with high accuracy, to the width of the intrinsic line-profile. Besides that, the opacity and emissivity stay isotropic in the comoving frame, because the velocity vanishes.
Therefore, we choose the Lagrangian frame for our numerical solution approach. But we have to transform the spherical symmetric RTE (2.26) into the Lagrangian frame by a Lorentz transformation.

Though the RTE in the Lagrangian frame offers physical and computational advantages, the cmf solution method we will present in chapter 3 is only working for monotonic velocity fields. However, the Lorentz transformation may only be applied if the relative velocity between the frames is uniform and constant. But in the case of an expanding atmosphere, the velocity field is of a radial form

$$\vec{v}(r) = v(r)\frac{\vec{r}}{r} \tag{2.27}$$

and hence, the expanding atmosphere is not an inertial frame. Each location in the atmosphere needs to be transformed into its own tangential inertial system which instantaneously coincide with the moving matter. Therefore, we need individual transformations for each point in the expanding atmosphere.

Furthermore, as the comoving frame is not an inertial frame, we shall leave the space time coordinates in the Eulerian frame, when we derive the cmf RTE. We thus avoid the need for a metric of an accelerated fluid frame [Castor 1972].

2.4.1 Lorentz Transformation of the Material and Radiation-Field Properties

The special theory of relativity describes the physical relations between inertial systems in the case of flat space-time. The appropriate mathematical formalism is described in the four-dimensional Minkowski real vector space. The relations between four-vectors in different inertial systems are determined by the *Lorentz transformation*. The general Lorentz transformation is described by a linear transformation of the form

$$x'^{\alpha} = \Lambda^{\alpha}_{\ \beta} x^{\beta} \tag{2.28}$$

In the case of two inertial systems moving relatively to each other with an arbitrarily directed velocity $\vec{\beta} = (\beta_x, \beta_y, \beta_z)$, the general Lorentz-Matrix is

$$\Lambda^i_{\ j} = \begin{pmatrix} \gamma & -\beta_x\gamma & -\beta_y\gamma & -\beta_z\gamma \\ -\beta_x\gamma & 1+(\gamma-1)\frac{\beta_x^2}{\beta^2} & (\gamma-1)\frac{\beta_x\beta_y}{\beta^2} & (\gamma-1)\frac{\beta_x\beta_z}{\beta^2} \\ -\beta_y\gamma & (\gamma-1)\frac{\beta_y\beta_x}{\beta^2} & 1+(\gamma-1)\frac{\beta_y^2}{\beta^2} & (\gamma-1)\frac{\beta_y\beta_z}{\beta^2} \\ -\beta_z\gamma & (\gamma-1)\frac{\beta_z\beta_x}{\beta^2} & (\gamma-1)\frac{\beta_z\beta_y}{\beta^2} & 1+(\gamma-1)\frac{\beta_z^2}{\beta^2} \end{pmatrix} \tag{2.29}$$

with the Lorentz factor $\gamma = 1/(1-\beta^2)^{1/2}$. At this point, we only know the static RTE (2.15) in the Eulerian frame. In the case of spherical symmetry, we derived the RTE in spherical coordinates. With time-dependence it is

$$\frac{1}{c}\frac{\partial I(\mu,\nu,t)}{\partial t} + \mu\frac{\partial I(\mu,\nu,t)}{\partial r} + \frac{(1-\mu^2)}{r}\frac{\partial I(\mu,\nu,t)}{\partial \mu} = \eta(\mu,\nu,t) - \chi(\mu,\nu,t)I(\mu,\nu,t) \tag{2.30}$$

For two inertial systems, the RTE is covariant and we can then easily replace the Eulerian physical quantities by their corresponding Lagrangian ones if we take in account the appropriate transformations and *relativistic invariant quantities*.

The Four-Momentum of a Photon

The angle cosine μ and the frequency ν are properties of the specific intensity $I(\nu,\mu)$. They describe the direction of propagation and the energy of a photon. These radiation-field properties

are combined in the four-momentum of the photon

$$\vec{p} = \begin{pmatrix} E/c \\ p_x \\ p_y \\ p_z \end{pmatrix} = \frac{h\nu}{c} \begin{pmatrix} 1 \\ n_x \\ n_y \\ n_z \end{pmatrix} \tag{2.31}$$

The four-momentum of the photon is a relativistic generalization in the Minkowski space. We get the relation between the properties of a photon in the Eulerian and Lagrangian frames by transforming the four-momentum according to (2.28)

$$p'^{\alpha} = \Lambda^{\alpha}_{\ \beta} \, p^{\beta}$$

With (2.29) and (2.31), we get the frequency and the direction of propagation in the comoving frame

$$\nu' = \nu\gamma \left(1 - \vec{\beta} \cdot \vec{n}\right) \tag{2.32}$$

$$\vec{n}' = \frac{\nu}{\nu'} \left[\vec{n} - \left(\gamma - \frac{\gamma - 1}{\beta^2} (\vec{\beta} \cdot \vec{n}) \right) \vec{\beta} \right] \tag{2.33}$$

Because we restrict the velocity field to the form (2.27), the dot product of $\vec{\beta}$ and $\vec{n}$ becomes

$$\vec{\beta} \cdot \vec{n} = \beta \, \vec{e}_r \cdot \vec{n}$$

$$= \beta\mu$$

From the differential operator (2.16) and (2.24), we know that

$$n_r = \frac{\partial r}{\partial s} = \mu$$

Thus we get the comoving angle cosine μ' from (2.33)

$$n'_r = \frac{\nu}{\nu'} \left[n'_r - \gamma\beta + \mu(\gamma - 1) \right]$$

$$\Leftrightarrow \mu' = \frac{\nu}{\nu'} \, \gamma \, (\mu - \beta)$$

and using (2.32) we get

$$\mu' = \frac{\mu - \beta}{1 - \beta\mu} \tag{2.34}$$

By the straightforward derivations of μ' and ν', we get the useful relations between the Eulerian and Lagrangian differentials

$$d\nu' = \left(\frac{\nu'}{\nu} \right) d\nu \tag{2.35}$$

$$d\mu' = \left(\frac{\nu}{\nu'} \right)^2 d\mu \tag{2.36}$$

which we will need for the formulation of the relativistic invariants.

The Relativistic Invariants

The relativistic invariants connect the quantities of the Eulerian and Lagrangian frames. We can determine these invariants from classical considerations. For the invariant of the specific intensity, we claim that the photon density will be maintained during the transformation. The number of photons N passing through an area dA perpendicular to $\vec{v}$ in the frequency intervall $[\nu, \nu + d\nu]$ into the solid angle $d\omega$ in direction $\vec{n}$ (with $d\vec{A} \cdot \vec{n} = \mu\ dA$) in the time intervall $[t, t + dt]$ has to be the same in both frames. If we choose the area dA to rest in the the stationary Eulerian frame, we find

$$N = \left[\frac{I(\mu, \nu)}{h\nu} \right]\ d\omega\ d\nu\ \mu\ dA\ dt$$

An observer in the comoving frame counts the same number of photons passing through the disk. When we consider the movement of dA in the comoving frame, the comoving observer counts

$$N' = \left[\frac{I'(\mu', \nu')}{h\nu'} \right]\ d\omega'\ d\nu'\ (dA\ \mu'\ dt' + c^{-1}\ dA\ v\ dt')$$

The first term gives the number of photons which would pass dA at rest, and the second term gives the number of photons which are *collected* by dA in the volume $(dA\ v\ dt')$ during its movement. The area dA is the same in both frames, because we claimed that $\vec{v}$ is perpendicular to dA. If we claim that

$$N' \stackrel{!}{=} N \tag{2.37}$$

we need the relations between the differentials of the Eulerian and Lagrangian frames from (2.35) and (2.36). Furthermore, we need the relations between the differentials of the solid angles and time. Because $d\omega = -d\mu\ d\phi$, the spherical symmetry $(d\phi' = d\phi)$ and the time dilatation, we find

$$\frac{d\omega'}{d\omega} = \frac{d\mu'}{d\mu} \tag{2.38}$$

$$dt' = \gamma\ dt \tag{2.39}$$

We can now write down (2.37) explicitly by using (2.34) to (2.39) and derive the invariant of the specific intensity

$$\frac{I}{I'} = \frac{\nu}{\nu'}\ \frac{d\omega'}{d\omega}\ \frac{d\nu'}{d\nu}\ \frac{dt'}{dt}\ \frac{1}{\mu}\ (\mu' + \beta)$$

$$= \frac{\nu}{\nu'}\ \left(\frac{\nu}{\nu'} \right)^2\ \frac{\nu'}{\nu}\ \gamma\ \frac{1}{\mu}\ (\mu' + \beta)$$

$$= \left(\frac{\nu}{\nu'} \right)^2\ \gamma\ \frac{1}{\mu}\ \left(\frac{\mu - \mu\beta^2}{1 - \beta\mu} \right)$$

$$\Leftrightarrow I(\nu, \mu) = \left(\frac{\nu}{\nu'} \right)^3\ I'(\mu', \nu') \tag{2.40}$$

For the invariant of the emissivity, we claim that the number of photons emitted from a certain volume dV into the solid angle $d\omega$ in the frequency intervall $(\nu, \nu + d\nu)$ in the time intervall $(t, t + dt)$ must be same in both frames

$$(\eta(\mu, \nu)\ d\omega\ d\nu\ dV\ dt)/h\nu = (\eta'(\mu', \nu')\ d\omega'\ d\nu'\ dV'\ dt')/h\nu'$$

Because the Lorentz contraction $(dx' = 1/\gamma \, dx)$ and the time dilatation effect $(dt' = \gamma dt)$ cancel each other out, the four-dimensional space time volume element $(dV \, dt)$ is the same in both frames and hence

$$\frac{\eta(\mu, \nu)}{\eta'(\mu', \nu')} = \frac{\nu}{\nu'} \frac{d\omega'}{d\omega} \frac{d\nu'}{d\nu}$$

$$\Leftrightarrow \eta(\mu, \nu) = \left(\frac{\nu}{\nu'}\right)^2 \eta'(\nu') \tag{2.41}$$

Here, we see explicitly that η' in the comoving frame is isotropic. Using (2.40) and (2.41), we conclude from the energy balance on the right hand side of the RTE that

$$\chi(\mu, \nu) = \left(\frac{\nu'}{\nu}\right) \chi'(\nu') \tag{2.42}$$

2.4.2 The Special Relativistic Radiative Transfer Equation

Substituting the invariants of the specific intensity (2.40), the emissivity (2.41) and the opacity (2.42) into the time-dependent, spherically symmetric RTE (2.30), we get

$$\eta'(\nu') - \chi'(\nu')I'(\mu', \nu') = \left(\frac{\nu}{\nu'}\right) \left[\frac{1}{c} \frac{\partial I'(\mu', \nu')}{\partial t} + \mu' \frac{\partial I'(\mu', \nu')}{\partial r} + \frac{1 - \mu^2}{r} \frac{\partial I'(\mu', \nu')}{\partial \mu}\right]$$

$$- 3\left(\frac{\nu}{\nu'^2}\right) \left[\frac{1}{c} \frac{\partial \nu'}{\partial t} + \mu \frac{\partial \nu'}{\partial r} + \frac{1 - \mu^2}{r} \frac{\partial \nu'}{\partial \mu}\right] I'(\mu', \nu') \, . \tag{2.43}$$

Equation (2.43) now contains the comoving frame intensity, emissivity and opacity, but we have to pay attention to the derivatives. Because the velocity of the matter in the atmosphere depends on the radius r and (in general) the time t, a variation of r or t causes a change of the velocity β and hence, μ' and ν' are not constant according to (2.34) and (2.32). Therefore, we have to take into account the variations of the comoving frame quantities μ' and ν' explicitly. By applying the chain rule, we can derive [Mihalas 1980]

$$\left.\frac{\partial}{\partial t}\right|_{r\mu\nu} = \left.\frac{\partial}{\partial t}\right|_{r\mu'\nu'} + \left.\frac{\partial \mu'}{\partial t}\right|_{r\mu\nu} \frac{\partial}{\partial \mu'} + \left.\frac{\partial \nu'}{\partial t}\right|_{r\mu\nu} \frac{\partial}{\partial \nu'} \, , \tag{2.44}$$

$$\left.\frac{\partial}{\partial r}\right|_{t\mu\nu} = \left.\frac{\partial}{\partial r}\right|_{t\mu'\nu'} + \left.\frac{\partial \mu'}{\partial r}\right|_{t\mu\nu} \frac{\partial}{\partial \mu'} + \left.\frac{\partial \nu'}{\partial r}\right|_{t\mu\nu} \frac{\partial}{\partial \nu'} \, , \tag{2.45}$$

$$\left.\frac{\partial}{\partial \mu}\right|_{rt\nu} = \left.\frac{\partial \mu'}{\partial \mu}\right|_{rt\nu} \frac{\partial}{\partial \mu'}\bigg|_{rt\nu} + \left.\frac{\partial \nu'}{\partial \mu}\right|_{t\mu\nu} \frac{\partial}{\partial \nu'} \, . \tag{2.46}$$

The first terms in (2.44) and (2.45) describe the explicit dependencies of the comoving quantities on the Eulerian space time coordinates. The second terms describe the implicit dependencies caused by the velocity field. The derivative of μ is only implicit, because μ' and ν' are isotropic in the comoving frame. We have to rewrite (2.43) so that it only contains comoving quantities except the Eulerian space time coordinates. We use the differential operator from (2.44), (2.45)

and (2.46), and after the straightforward derivation of the comoving quantities, we get

$$\eta'(\nu') - \chi'(\nu')I'(\mu',\nu') = \frac{\gamma}{c}(1+\beta\mu')\frac{\partial I'(\mu',\nu')}{\partial t} + \gamma(\mu'+\beta')\frac{\partial I'(\mu',\nu')}{\partial r}$$

$$+ \gamma(1-\mu'^2)\left[\frac{1+\beta\mu'}{r} - \frac{\gamma^2}{c}(1+\beta\mu')\frac{\partial\beta}{\partial t} - \gamma^2(\mu'+\beta)\frac{\partial\beta}{\partial r}\right]\frac{\partial I'(\mu',\nu')}{\partial\mu'}$$

$$- \gamma\left[\frac{\beta(1-\mu'^2)}{r} + \frac{\gamma^2}{c}\mu'(1+\beta\mu')\frac{\partial\beta}{\partial t} + \gamma^2\mu'(\mu'+\beta)\frac{\partial\beta}{\partial r}\right]\nu'\frac{\partial I'(\mu',\nu')}{\partial\nu'}$$

$$+ 3\gamma\left[\frac{\beta(1-\mu'^2)}{r} + \frac{\gamma^2}{c}\mu'(1+\beta\mu')\frac{\partial\beta}{\partial t} + \gamma^2\mu'(\mu'+\beta)\frac{\partial\beta}{\partial r}\right]I'(\mu',\nu')$$

$$(2.47)$$

Equation (2.47) is called the *spherical symmetric special relativistic radiative transfer equation* (SSRTE). Because we are not interested in the time dependence, we can drop it and the SSRTE becomes

$$\eta'(\nu') - \chi'(\nu')I'(\mu',\nu') = \gamma(\mu'+\beta')\frac{\partial I'(\mu',\nu')}{\partial r}$$

$$+ \gamma(1-\mu'^2)\left[\frac{1+\beta\mu'}{r} - \gamma^2(\mu'+\beta)\frac{\partial\beta}{\partial r}\right]\frac{\partial I'(\mu',\nu')}{\partial\mu'}$$

$$- \gamma\left[\frac{\beta(1-\mu'^2)}{r} + \gamma^2\mu'(\mu'+\beta)\frac{\partial\beta}{\partial r}\right]\frac{\partial(\nu' I'(\mu',\nu'))}{\partial\nu'}$$

$$+ 4\gamma\left[\frac{\beta(1-\mu'^2)}{r} + \gamma^2\mu'(\mu'+\beta)\frac{\partial\beta}{\partial r}\right]I'(\mu',\nu')\,.\qquad(2.48)$$

Because during the numerical solution of the SSRTE we will work with a wavelength discretization instead of frequencies, we replace ν' in (2.48) with λ'. The frequency and wavelength descriptions are equivalent and the SSRTE does not change except the derivative of I' with respect to ν'. Because

$$d\lambda' = -\frac{1}{\nu'^2}d\nu'$$

the sign of the $\frac{\partial(\nu' I')}{\partial\nu'}$ changes, and the time independent SSRTE becomes

$$a_r\frac{\partial I'_\nu}{\partial r} + a_\mu\frac{\partial I'_\nu}{\partial\mu'} + a_\lambda\frac{\partial\lambda I'_\nu}{\partial\lambda'} + 4a_\lambda I'_\nu = \eta'_\nu - \chi'_\nu I'_\nu\qquad(2.49)$$

with the coefficients

$$a_r = \gamma(\mu'+\beta)$$

$$a_\mu = \gamma(1-\mu'^2)\left[\frac{1+\beta\mu'}{r} - \gamma^2(\mu'+\beta)\frac{\partial\beta}{\partial r}\right]$$

$$a_\lambda = \gamma\left[\frac{\beta(1-\mu'^2)}{r} + \gamma^2\mu'(\mu'+\beta)\frac{\partial\beta}{\partial r}\right]$$

In the following, we will drop the explicit dashed notation of the cmf quantities because from now on, we describe the RTE in the comoving frame unless otherwise noted.

Again, though equation (2.49) describes the radiative transfer in a comoving frame, though as a whole, a spherically expanding atmosphere is not an inertial system. The SSRTE describes the radiative transfer in a tangential inertial system in (r, Θ, Φ) moving with $\beta(r)\vec{e}_r(\Theta, \Phi)$, which instantaneously coincide with the moving matter. Hence, to describe radiative transfer through layers of different velocities, we follow and discretize the way of a photon through the atmosphere and transform its properties into the comoving frame individually at each discretization point.

2.5   Line Transitions

The implementation of the numerical solution scheme we present in the following chapter needs to be tested seriously. For that, we computed a series of line transitions for a hypothetic two-level atom. The atom in this model consists of only two levels l and u, between which radiative and collisional transitions can occur. Of course, this model is not very realistic, but it provides an adequate description for *resonance lines* that originate from ground state transitions. Furthermore, the two-level model provides an excellent possibility for a testing environment, because it allows us to determine the dependency of our solution on the wavelength coupling in the SSRTE.

2.5.1   The Einstein Relations for Bound-Bound Transitions

We describe the emission and absorption rates between the lower level l and the upper level u statistically by introducing the Einstein rate coefficients. We consider the following processes:

Radiative Excitation

Radiative Excitation describes the direct absorption of a photon which leads to an upward transition from level l to u. The rate of this process for radiation of specific intensity I_ν can be described by the Einstein coefficient B_{lu}

$$n_l(\nu)R_{lu}(d\omega/4\pi) = n_l(\nu)B_{lu}I_\nu(d\omega/4\pi) \qquad (2.50)$$

where $n_l(\nu)$ is the number of atoms per cm^3 in state l which can absorb radiation at frequencies on the range $(\nu, \nu+d\nu)$. The spectrum line in general is not sharp because of various perturbation effects in a stellar atmosphere. For example, nearby atoms, ions and molecules shift the energy levels l and u slightly due to electromagnetic interactions so that the transition energy is not sharp. Furthermore, the uncertainty principle connects the finite lifetime of the state u with an uncertainty in energy and causes the natural or intrinsic linewidth.
Thus the transition is not a sharp line but is described by an *absorption profile* ϕ_ν. It describes the dependency of $n_l(\nu) = n_l\phi_\nu$ on the frequency ν, where n_l is the total number of atoms in state l. It is normalized so that $\int \phi_\nu d\nu = 1$. The transition energy between the levels l and u is given by $E_u - E_l = h\nu_{ul}$. We can then describe the rate, at which energy is removed from a beam, by a macroscopic true absorption coefficient a_ν

$$a_\nu I_\nu = n_l(B_{lu}h\nu_{lu}/4\pi)\phi_\nu I_\nu \qquad (2.51)$$

where a_ν now describes the true absorption which is not corrected for stimulated emission (in contrast to χ_ν).

Spontaneous and Induced Radiative Deexcitation

There are two possible radiative processes when the excited atom returns from the upper level u to the lower level l. The first one is the *spontaneous emission* of a photon. The Einstein coefficient A_{ul} denotes the probability per unit time for an excited atom to deexcite by spontaneous emission. The rate of energy emitted by spontaneous emission is described by

$$\eta_\nu(\text{spontaneous}) = n_u(A_{ul}h\nu_{lu}/4\pi)\psi_\nu \tag{2.52}$$

with the *emission profile* ψ_ν and the total number of excited atoms n_u.
The second possibility is the *induced emission*. The probability per unit time is described by the Einstein coefficient B_{ul}. The rate of emitted energy by induced deexcitation becomes

$$\eta_\nu(\text{induced}) = n_u(B_{ul}h\nu_{lu}/4\pi)\psi_\nu I_\nu \tag{2.53}$$

We noted explicitly that the emission profiles for spontaneous and induced emission are the same as can be shown in quantum mechanics. It is important to notice that the energy emitted by induced emission is proportional to and has the same angular distribution as the incident specific intensity I_ν. That is why spontaneous emission is sometimes considered as negative extinction. In fact, this is not quite correct, because in general, the absorption profile ϕ_ν and the emission profile ψ_ν are not the same.

Collisional Excitation and Deexcitation

In contrast to the radiative excitation and deexcitation processes, collisional processes change the states of atoms without absorbing or emitting photons. There is a wide variety of possible collisions that may occur between the atoms, ions and electrons in the plasma of a stellar atmosphere. But since in thermodynamic equilibrium the velocities of the electrons are a factor of $(m_H A/m_e)^{\frac{1}{2}}$ larger than those of ions of atomic weight A, we only consider electron collisions causing a transition from state l to u with the rate

$$n_l C_{lu} = n_l n_e \int_{v_0}^\infty \sigma_{lu}(v) v f(v) dv \tag{2.54}$$

with n_e denoting the electron density, σ_{lu} the electron collision cross-section, $f(\nu)$ the normalized velocity distribution and v_0 the threshold velocity with $1/2mv_o^2 = h\nu_0$.

Einstein Relations

The Einstein coefficients are coupled by the Einstein relations. These are derived from the calculation of the absorption and emission rates in thermodynamic equilibrium (TE). In this case, the occupation numbers in TE n_l^* and n_u^* are determined by the Boltzmann law

$$\frac{n_u^*}{n_l^*} = \frac{g_u}{g_l} \ \exp(-h\nu_{ul}/kT) \tag{2.55}$$

where g_l and g_u are the statistical weights of the lower and upper levels. In a TE situation, emission and absorption processes have to be balanced, and the emission and absorption profiles

are the same. With the use of the Planck function for the emitted energy, we derive the Einstein relations

$$g_l B_{lu} = g_u B_{ul} \qquad A_{ul} = (2h\nu^2/c^2) B_{ul}$$

$$n_l^* C_{lu} = n_u^* C_{ul}$$

which are important for the formulation of the line source function. Although the Einstein relations are derived for the TE case, they describe the statistical properties of an atom itself. Therefore they have to be independent from the radiation field and must be valid in general.

2.5.2 The Source Function for the Two-Level Atom

For the formulation of the line source function, we consider only absorption and emission processes from the line itself. We neglect the contributions from the continuum. The extinction coefficient can then be described with the Einstein coefficients by accounting for the stimulated emission rates as a negative contribution. The emissivity is determined by spontaneous emission processes

$$\chi_\nu = (n_l B_{lu} - n_u B_{ul})(h\nu/4\pi) \qquad \eta_{ul} = n_u A_{ul}(h\nu/4\pi)$$

We assumed *complete redistribution* so that the emission and absorption profiles are equal. Now we can obtain an expression for the line source function by using the Einstein relations

$$S_l = \frac{n_u A_{ul}}{n_l B_{lu} - n_u B_{ul}} = (2h\nu^3/c^2)\left[(n_l g_u/n_u g_l) - 1\right]^{-1} \tag{2.56}$$

Equation (2.56) is called the *frequency-independent* source function, because the line profile ϕ_ν is usually sharped peaked. Therefore, the factor ν^3 only varies slightly over the profile. Here, S_l in given in an implicit form, because the occupation numbers n_u and n_l depend on the radiation field.

By using the equations of statistical equilibrium, we can derive an explicit term for the line source function. In the case of statistical equilibrium, the total amount of radiative and collisional excitation and deexcitation rates have to be identical

$$n_l \left(B_{lu} \int \phi_\nu J_\nu \, d\nu + C_{lu} \right) = n_u \left(A_{ul} + B_{ul} \int \phi_\nu J_\nu \, d\nu + C_{ul} \right) \tag{2.57}$$

We can now obtain an expression for the quotient of the occupation numbers n_l/n_u by the Einstein coefficients. The line source function becomes

$$S_l = \frac{\int \phi_\nu J_\nu \, d\nu + \epsilon' B_\nu}{1 + \epsilon'} \equiv (1 - \epsilon)\bar{J}_\nu + \epsilon B_\nu \tag{2.58}$$

with

$$\epsilon' \equiv C_{ul}(1 - e^{(-h\nu/kT)})/A_{ul}$$

$$\epsilon \equiv \frac{\epsilon'}{1 + \epsilon'}$$

In equation (2.58) we noted the line source function in a form we already know from the coherent source function (2.10). But in contrast to the coherent source function the line source function S_l now contains a *non-coherent* scattering term $\bar{J}_\nu$. It describes the energy transported to the

region of interest from all over the atmosphere by continuous scattering processes. The thermal source part $\epsilon' B_\nu$ describes the energy emitted by local radiative deexcitation.

It is interesting to notice that in the case of large densities the collisional Einstein coefficient C_{ul} will obviously dominate and ϵ' becomes $\gg 1$. Then we get an LTE situation with $S_l \approx B_\nu$. However, in the outer regions where observable line formation takes place, the atmosphere is optically thin and ϵ' becomes $\ll 1$. The source function will then dramatically differ from the Planck function.

Chapter 3

The Solution of the Equation of Radiative Transfer

In this chapter we describe the basics of numerical radiative transfer which is crucial for solving the RTE. We describe the numerical methods we use for solving the RTE, especially the Λ iteration scheme and the operator splitting method.

3.1   Introduction

This chapter presents the solution methods we are using to solve the SSRTE (2.49). It is based on the 1D solution method described in [Mihalas 1980] which we extend in order to solve the radiative transfer problem in 3D. In section (2.3.1), we derived a formal solution (2.21) of the basic RTE (2.19). But to calculate the formal solution, we need to know the source function. We know this already as the scattering problem (section 2.2) and it is caused by the non-locality (section 2.7) of the interaction processes between radiation and matter. However, for highly opaque atmospheres, it is possible to solve the RTE analytically and find consistent solutions of the source function and the radiation field. This is possible, when the mean free path of a photon is short relative to the gradient of the temperature structure of the atmosphere. In this case, the radiation field is dominated by the local thermodynamic properties, because a photon is not able to transport energy far between layers of different thermodynamic properties. Thus, we can assume an atmosphere determined by an LTE situation. The source function is then determined by the local thermal emission (2.12), and we can solve the RTE with the formal solution (2.21).

The problem with the LTE assumption is that we neglect any global interaction processes of the radiation field with the matter. Especially in the outer regions of a star, where the atmosphere becomes optically thin and light can leave the star, any assumptions of thermodynamic equilibrium becomes inaccurate. In these areas the propagation of a photon is not any more dominated by thermal but by scattering processes. Therefore, the scattering contribution of the source function becomes important (2.10), and we need to find consistent solutions of the integro-differential RTE (2.20).

In the NLTE situation, an analytical approach of solving the RTE is limited due to the non-linearity of the transfer problem (section 2.3). However, most of the analytical approaches originate in the pre-computer era. With the power of modern computers, we are no longer forced to make simplifying assumptions to obtain analytical approximations. We are able to verify and approve the theory behind the model atmosphere for a variety of realistic astronomical objects.

The numerical approach is based on finding consistent solutions of the source function and the the mean intensity by iterative methods. This is a demanding task, because it is not trivial to find a fast converging iteration scheme. The demand of computational power and memory of the 3D radiative transfer solution even pushes the envelope of modern supercomputers. Parallel computing and well-considered memory management are essential in the process of implementing computational solution methods [Hauschildt and Baron 2006].

3.2   Modeling Atmospheres in PHOENIX

PHOENIX is a scientific computer code for the computation of model atmospheres. It can calculate atmospheres and spectra of stars and planets, including main sequence stars, giants, white dwarfs, stars with winds, TTauri stars, Novae, Supernovae, brown dwarfs and extrasolar giant planets. The goal of the PHOENIX code is to construct self-consistent model atmospheres. The mathematical model describes the physical dependencies of the atmosphere on some fundamental physical quantities which characterize the atmosphere. PHOENIX uses the temperatures T, the gas pressures P_{gas} and the population numbers n at each discrete point in the atmosphere as fundamental variables. These variables are connected (mostly non-linearly) in the following basic equations which describe the dynamics of the atmosphere

- hydrodynamic equilibrium

- equation of state

- rate equations

- radiative transfer equation

- radiative equilibrium

The fundamental variables determine a lot of additional physical quantities which determine the structure and dynamics of the atmosphere, e.g., the densities, the population densities and the specific and mean intensities. To construct a self-consistent model atmosphere, we have to find sets of fundamental variables determining a physical structure of the atmosphere, which fulfils the basic equations (Figure 3.1).
To find a set of consistent physical quantities, PHOENIX uses a scheme of nested iterative solutions. This solution scheme accounts for the strong couplings between important physical variables directly and iteratively for the indirect couplings between variables. The problem of constructing a consistent model atmosphere is then reduced to a number of smaller problems. By this, PHOENIX uses the fact that the level of coupling between the variables is different [Hauschildt and Baron 1999].

From (Figure 3.1) we can see that the solution of the radiative transfer equation, which is the topic of this thesis, is only one small step in the problem of finding a self-consistent model atmosphere. Nevertheless, it is a crucial one, because the radiative transfer equation allows us to account for the global couplings of physical variables in the case of NLTE.
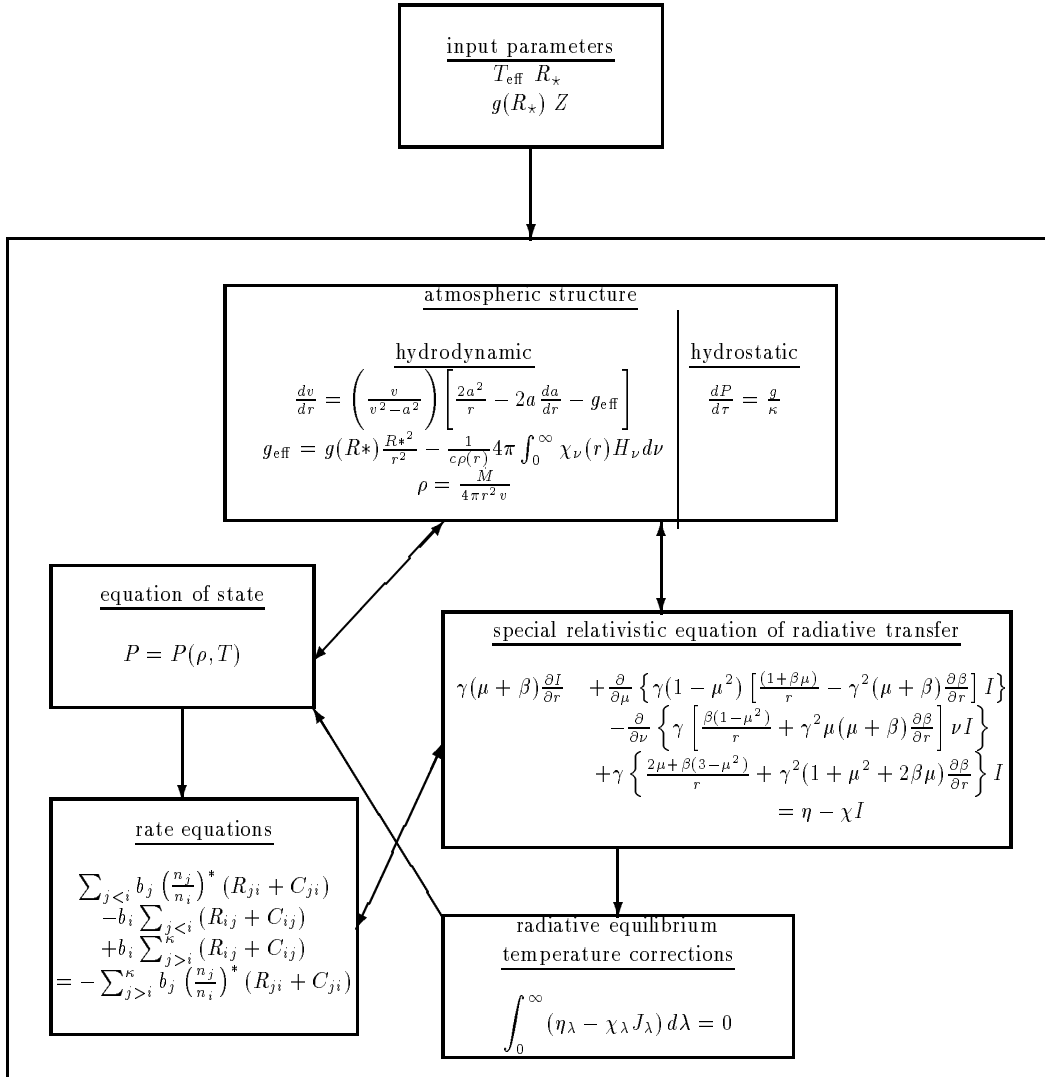
PHOENIX REALWIND

Figure 3.1: The PHOENIX flowchart; It describes the relations between (some of) the mathematical equations which describe the physics of an atmosphere. In order to calculate a model atmosphere, we have to find consistent solutions of all equations. Unfortunately, most of the dependencies are non-linear (from [Hauschildt and Baron 1999], by courtesy of Peter H. Hauschildt).

3.3   The Method of Characteristics

The idea of the method of characteristics is to reduce a partial differential equation (PDE) to a parameterized ordinary differential equation (ODE). The parameter describes a *characteristic* curve along which the PDE becomes an ODE which can be solved by piecewise integration along the characteristic. If we find solutions for all initial conditions of the ODE, we can solve the original PDE. This is called the *method of characteristics* [Olson and Kunasz 1987].

In the case of the SSRTE (2.49), we have to find the characteristics of the radiation field. These can be interpreted as the paths of photons of a certain wavelength which are travelling through the atmosphere (Figure 3.2). For a static atmosphere, the characteristics are straight lines because for an observer in an inertial frame, the optical path is always straight. For an observer in a comoving frame in a certain layer of the atmosphere, the optical path is straight as well. But because of the different velocities of the layers in the atmosphere, a photon experiences continuous wavelength shifts, and the way of a photon of a fixed wavelength seems to be curved. In fact, there is no frame in which this curvature is observable because for an observer in a single tangential comoving inertial frame, the optical path is still straight. The curvature is an effect of continuous Lorentz transformations between the Eulerian frame and the Lagrangian frames the photon passes on its way through the atmosphere.
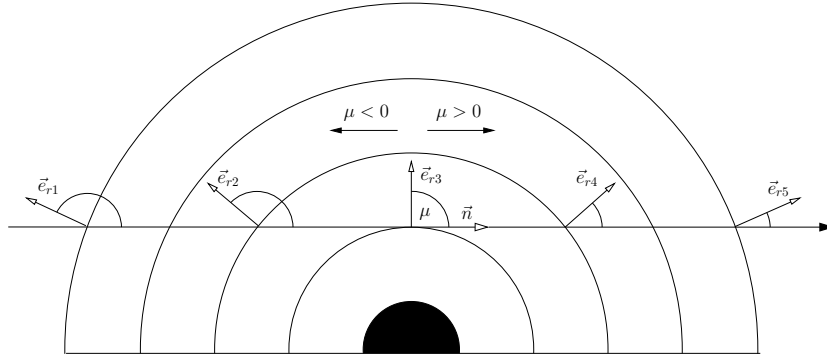

Figure 3.2: The geometrical situation of a photon travelling through different layers of an atmosphere in the Eulerian frame; each layer is crossed under an individual angle given by $\mu(\Theta, \Phi, \vec{n}) = \vec{e}_r(\Theta, \Phi) \cdot \vec{n}$. When the angle cosine is known in the Eulerian frame, it can easily be transformed into a tangential Lagrangian frame according to (2.34).

We introduce the parameterization by the line element ds which describes an infinitesimal movement of a photon in the atmosphere. We then define the total derivative of I with respect to s as

$$\frac{dI}{ds} = \frac{dr}{ds}\frac{\partial I}{\partial r} + \frac{d\mu}{ds}\frac{\partial I}{\partial \mu} \tag{3.1}$$

The comparison with (2.49) gives us the definition of the characteristic rays

$$\frac{dr}{ds'} = a_r = \gamma(\mu + \beta) = n_r' \frac{\partial r}{\partial r'} \tag{3.2}$$

$$\frac{d\mu}{ds'} = a_\mu = \gamma(1-\mu^2)\left[\frac{1+\beta\mu}{r} - \gamma^2(\mu+\beta)\frac{\partial\beta}{\partial r}\right] = -\sin\theta\, n_\theta' \frac{\partial\theta}{\partial\theta'} \tag{3.3}$$

With (3.2) and (3.3) we can now reduce the partial differential SSRTE to a more simple form. (2.49) becomes

$$\frac{dI_\lambda}{ds} + a_\lambda \frac{\partial \lambda I_\lambda}{\partial \lambda} = \eta_\lambda - (\chi_\lambda + 4a_\lambda)I_\lambda \ . \tag{3.4}$$

Equation (3.4) is still a PDE but with a parameterization of the spatial derivatives. To solve (3.4) we have to discretize the differential quotients and convert it to a form like (2.19). Then we can solve (3.4) by a piecewise integration of the formal solution (2.21).

In general, the line element ds must be calculated for the comoving frame. That is important to remember, because now, we lost all explicit connections to the Eulerian space coordinates in the parameterized radiative transfer equation (3.4). The relations to the Eulerian frame are given by (3.2) and (3.3). However, we must explicitly calculate ds by a Lorentz transformation of the Eulerian space coordinates (section 3.5).

3.4 Discretization of the Radiative Transfer Equation

Because the SSRTE (3.4) has a spatial and a wavelength dependency, we have to solve it numerically on a discrete spatial and wavelength grid. The wavelength grid has to be ordered because we will need the solutions of the previous wavelength point for the actual solution of the RTE (section 3.4.1). For the spatial grid, the volume of the atmosphere is divided into discrete elements of space (Figure 3.3). Such a finite element of space is also called a volume element or *voxel*. Each voxel is then assigned its physical quantities like opacity, emissivity, intensity, source function and many more. The number of discretization elements, also called *resolution*, determines the accuracy of the model atmosphere. In the case of the SSRTE (3.4), we already simplified the solution of the spatial derivative to the solution along characteristic rays. The line element ds in the Eulerian frame is then discretized on the voxel grid by

$$ds \approx \Delta s = |s_i - s_{i-1}| \ , \tag{3.5}$$

where s_i is a discretization point on the characteristic. The finite line difference Δs allows us to compute the monochromatic formal solution (2.21) by a piecewise integration along the characteristic ray if we know the opacities, the source function and the initial values (intensities at the outer or inner boundaries of the atmosphere). The formal solution on a discretized characteristic then becomes

$$I(\tau_i) = I(\tau_{i-1}) \ \exp{(\tau_{i-1} - \tau_i)} + \int_{\tau_{i-1}}^{\tau_i} S(\tau) \ e^{(\tau - \tau_i)} d\tau \tag{3.6}$$

$$= I_{i-1} \ \exp{(-\Delta \tau_{i-1})} + \Delta I_i \tag{3.7}$$

where $\Delta \tau_i$ is a finite optical depth element given by a piecewise linear interpolation

$$\Delta \tau_i = \frac{1}{2}(\chi_{i-1} + \chi_i)\Delta s$$

χ_i is the opacity at the discretization point s_i on the characteristic and is given by the physical quantities of the voxel the characteristic hits at s_i. The integral in (3.6) is solved analytically by a linear or parabolic interpolation of the source function

$$\Delta I_i = \alpha_i S_{i-1} + \beta_i S_i + \gamma_i S_{i+1} \tag{3.8}$$

In the case of linear interpolation the γ-coefficient is zero. The coefficients α_i, β_i and γ_i depend on the optical depths between s_{i-1} and s_{i+1}. They are given in [Olson *et al.* 1986].

The SSRTE (3.4) and the formal solution (3.6) do not contain dependencies on solid angles because of the parameterization of the characteristics. We did this, because we know that a photon is propagating through the spatial grid according to (3.2) and (3.3). By this, we simplified the 3D transfer problem to a 1D solution along characteristics. However, the 3D information of the specific intensity is recovered by many initial directions of the characteristics. As we chose the atmosphere to be described in spherical coordinates, a single characteristic hits the voxels of the grid under different angles $\vec{n} \cdot \vec{e}_r$ (Figure 3.2) and thus, it has different contributions to the angular resolution of the mean intensity in the different layers. To calculate the mean intensity J_ν in 3D radiative transfer, we need an appropriate discrete angular resolution of the specific intensity at each voxel. Therefore, we need each voxel to be passed by characteristics of all directions on the solid angle grid. We can then compute the mean intensity at each voxel by a numerical quadrature.
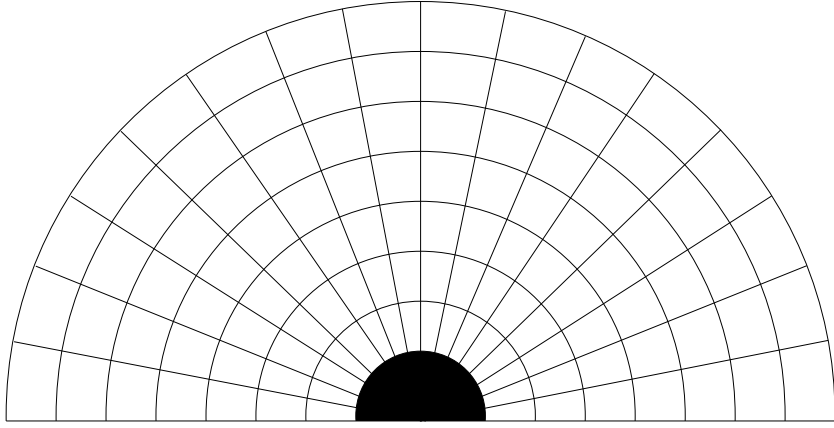

Figure 3.3: The atmosphere is approximated by a spherical voxel grid.

3.4.1 Wavelength Discretization

The formal solution (3.6) is only valid for a static atmosphere, where the RTE is of the form (section 2.3)

$$\frac{dI_\lambda}{ds} = I_\lambda - S_\lambda \tag{3.9}$$

We have to bring (3.4) into the form of (3.9). Thus, we have to discretize the wavelength dependent differential quotient in (3.4) by approximating it with a difference quotient on a wavelength grid. According to [Hauschildt and Baron 2004], this is done by

$$\left.\frac{\partial \lambda I_\lambda}{\partial \lambda}\right|_{\lambda=\lambda_l} \approx \frac{\lambda_l I_{\lambda_l} - \lambda_{l-1} I_{\lambda_{l-1}}}{\lambda_l - \lambda_{l-1}} \tag{3.10}$$

Here, I_{λ_l} is the specific intensity at the point λ_l on the wavelength grid. We have two different choices for the wavelength discretization. We can insert (3.10) before the definition of the

comoving frame opacity. By this, one part of the wavelength derivative becomes an additional contribution to the opacity. The other part is included in the definition of the comoving frame source function.

On the other hand, when we first define the comoving frame opacity and defer the wavelength discretization (3.10), the whole derivative can be considered as an additional source term. It is possible to mix both discretization schemes via a Crank-Nicholson scheme to remove numerical instabilities. We introduce both discretization schemes and mix them afterwards.

First Discretization

We insert (3.10) into the SSRTE (3.4) and get the wavelength-discretized SSRTE

$$\frac{dI_\lambda}{ds} + a_\lambda \frac{\lambda_l I_{\lambda_l} - \lambda_{l-1} I_{\lambda_{l-1}}}{\lambda_l - \lambda_{l-1}} = \eta_{\lambda_l} - (\chi_{\lambda_l} + 4a_{\lambda_l}) I_{\lambda_l}$$

$$\Leftrightarrow \frac{dI_\lambda}{ds} + a_\lambda \frac{\lambda_{l-1}}{\lambda_l - \lambda_{l-1}} I_{\lambda_{l-1}} = \eta_{\lambda_l} - \left[\chi_{\lambda_l} + a_{\lambda_l} \left(4 + \frac{\lambda_l}{\lambda_l - \lambda_{l-1}} \right) \right] I_{\lambda_l} \quad (3.11)$$

We can now define the comoving frame optical depth with the comoving frame opacity $\hat{\chi}$

$$\begin{aligned} d\tau =& \ - \left[\chi_{\lambda_l} + a_{\lambda_l} \left(4 + \frac{\lambda_l}{\lambda_l - \lambda_{l-1}} \right) \right] \quad ds \\ \equiv& \qquad\qquad -\hat{\chi}_{\lambda_l} \qquad\qquad ds \end{aligned} \quad (3.12)$$

We defined the optical depth in (2.18) with a negative sign, because the line element ds gets negative when we are going downwards into an atmosphere. The two signs then cancel out each other, and the opacity increases inwards. During numerical calculations along a characteristic, ds is approximated by Δs according to (3.5) which is always positive. Thus, we do not need the negative sign, when we calculate the optical depth during the numerical solution. However, we keep it here for formal reasons because ds is infinitesimal. In fact, the formal solution does not depend on the direction which is defined by a negative or positive ds. With (3.12) the RTE (3.11) becomes

$$\frac{dI_\lambda}{d\tau} = I_{\lambda_l} - \frac{\chi_{\lambda_l}}{\hat{\chi}_{\lambda_l}} \left(S + \frac{a_\lambda}{\chi} \frac{\lambda_{l-1}}{\lambda_l - \lambda_{l-1}} I_{\lambda_{l-1}} \right)$$

$$\equiv I - \hat{S} \quad (3.13)$$

Additionally to the static source function S, the comoving frame source function $\hat{S}$ now contains a wavelength dependent part which is caused by the velocity field. The optical depth (3.12) also contains effects of the wavelength derivative and becomes very large in comparison to the static optical depth χ. We can solve (3.13) by applying the formal solution (3.7).

Second Discretization

By inserting the discretization (3.10) directly into the RTE, the optical depth becomes dependent on the wavelength derivative. We can also define an optical depth which is independent of the wavelength derivative by deferring the discretization and defining the optical depth as

$$\begin{aligned} d\tau =& \ -(\chi_{\lambda_l} + 4a_\lambda) \quad ds \\ \equiv& \qquad -\hat{\chi}_{\lambda_l} \qquad ds \end{aligned} \quad (3.14)$$

The RTE (3.4) becomes

$$\frac{dI_{\lambda_l}}{d\tau} = I_{\lambda_l} - \frac{\chi_{\lambda_l}}{\hat{\chi}_{\lambda_l}} S_{\lambda_l} - \frac{-a_\lambda}{\hat{\chi}_{\lambda_l}} \frac{\partial \lambda I_\lambda}{\partial \lambda} \tag{3.15}$$

$$\equiv I_{\lambda_l} - \hat{S}_{\lambda_l} - \tilde{S}_{\lambda_l} \tag{3.16}$$

The wavelength derivative is completely part of a new source term which describes the effects of the velocity field. The RTE (3.16) can be solved by discretizing the wavelength derivative in the additional source term $\hat{S}$ and applying the formal solution (3.7) by splitting the integral into two terms. The formal solution then becomes

$$I_{i,l} = I_{i-1,l}\, e^{-\Delta\tau_{i-1,l}} + \Delta\hat{I}_{i,l} + \Delta\tilde{I}_{i,l} \tag{3.17}$$

$$\text{with} \quad \Delta\hat{I}_{i,l} = \alpha_{i,l}\hat{S}_{i-1,l} + \beta_{i,l}\hat{S}_{i,l} + \gamma_{i,l}\hat{S}_{i+1,l}$$

$$\Delta\tilde{I}_{i,l} = \tilde{\alpha}_{i,l}\tilde{S}_{i-1,l} + \tilde{\beta}_{i,l}\tilde{S}_{i,l} \tag{3.18}$$

$$\hat{S}_{i,l} = \frac{\chi_{i,l}}{\hat{\chi}_{i,l}} S_{i,l}$$

$$\tilde{S}_{i,l} = -\frac{a_{i,l}}{\hat{\chi}_{i,l}} \left.\frac{\partial \lambda I}{\partial \lambda}\right|_{i,l} \tag{3.19}$$

The indices i and l refer to a spatial grid point s_i on the characteristic and a point λ_l on the wavelength grid. The integration of $\tilde{S}$ is done by using linear interpolation, because we restrict our solution scheme to monotonically increasing or decreasing velocity fields. By this, we avoid the need to solve a matrix equation [Knop *et al.* 2007] [Chen *et al.* 2007].

We carry out the wavelength discretization by using (3.10) and deriving

$$\left.\frac{\partial \lambda I_\lambda}{\partial \lambda}\right|_{i,l} = \frac{\lambda_l}{\lambda_l - \lambda_{l-1}} I_{i,l} - \frac{\lambda_{l-1}}{\lambda_l - \lambda_{l-1}} I_{i,l-1}$$

By inserting the discretization into the definition of $\tilde{S}$ (3.19), we can rewrite the integral (3.18) as

$$\Delta\tilde{I}_{i,l} = \tilde{\alpha}_{i,l} \left[-\frac{a_{i-1,l}}{\hat{\chi}_{i-1,l}} \left(\frac{\lambda_l}{\lambda_l - \lambda_{l-1}} I_{i-1,l} - \frac{\lambda_{l-1}}{\lambda_l - \lambda_{l-1}} I_{i-1,l-1} \right) \right]$$

$$+ \tilde{\beta}_{i,l} \left[-\frac{a_{i,l}}{\hat{\chi}_{i,l}} \left(\frac{\lambda_l}{\lambda_l - \lambda_{l-1}} I_{i,l} - \frac{\lambda_{l-1}}{\lambda_l - \lambda_{l-1}} I_{i,l-1} \right) \right]$$

By defining the coefficients

$$p_{i-1,l} = -\frac{a_{i-1,l}}{\hat{\chi}_{i-1,l}} \frac{\lambda_l}{\lambda_l - \lambda_{l-1}}$$

$$p_{i-1,l-1} = -\frac{a_{i-1,l}}{\hat{\chi}_{i-1,l}} \frac{\lambda_{l-1}}{\lambda_l - \lambda_{l-1}}$$

$$p_{i,l} = -\frac{a_{i,l}}{\hat{\chi}_{i,l}} \frac{\lambda_l}{\lambda_l - \lambda_{l-1}}$$

$$p_{i,l-1} = -\frac{a_{i,l}}{\hat{\chi}_{i,l}} \frac{\lambda_{l-1}}{\lambda_l - \lambda_{l-1}}$$

we can finally rewrite the formal solution (3.17) as

$$(1 - \tilde{\beta}_{i,l}\,p_{i,l})I_{i,l} = (\tilde{\alpha}_{i,l}\,p_{i-1,l} + \exp\left(-\Delta\tau_{i,1}\right))I_{i-1,l}$$

$$- \tilde{\alpha}_{i,l}\,p_{i-1,l-1}\,I_{i-1,l-1} - \tilde{\beta}_{i,l}\,p_{i,l-1}\,I_{i,l-1}$$

$$+ \Delta\hat{I}_{i,l} \tag{3.20}$$

Equation (3.20) describes a recursive solution for the RTE (3.4). It can be calculated along a characteristic with the appropriate initial values. The actual specific intensity $I_{i,l}$ on an arbitrary point on the characteristic depends on the previous intensity $I_{i-1,l}$ on the spatial grid at the same wavelength point and the previous and actual intensities $I_{i-1,l-1}$ and $I_{i,l-1}$ on the spatial grid of the previous wavelength point (Figure 3.4).

Combination of the Discretization Schemes

The two discretization schemes show different behavior in 1D radiative transfer [Hauschildt and Baron 2004]. The deferred discretization scheme is accurate to second order in $\Delta\lambda$. It is more accurate than the first method. But under certain circumstances, the deferred scheme can become numerically instable. This instability appears as oscillations on the edges of spectral lines, but it can be removed by a combination of both discretization methods via a Crank-Nicholson scheme. We introduce the factor $\xi \in [0,1]$ which controls the mix between the two discretization schemes. The comoving frame opacity and source functions then become

$$\hat{\chi}_{\lambda_l} = \left[\chi_{\lambda_l} + a_{\lambda_l}\left(4 + \xi\frac{\lambda_l}{\lambda_l - \lambda_{l-1}}\right)\right]$$

$$\hat{S}_{\lambda_l} = \frac{\chi_{\lambda_l}}{\hat{\chi}_{\lambda_l}}\left(S + \xi\frac{a_{\lambda_l}}{\chi_{\lambda_l}}\frac{\lambda_{l-1}}{\lambda_l - \lambda_{l-1}}I_{\lambda_{l-1}}\right)$$

$$\tilde{S}_{\lambda_l} = -(1-\xi)\frac{a_{\lambda_l}}{\hat{\chi}_{\lambda_l}}\frac{\partial\lambda I}{\partial\lambda}\bigg|_{\lambda=\lambda_l}$$

For $\xi = 1$, we get the first discretization definitions and for $\xi = 0$, we get the deferred ones. For both cases, we can use the recursive formal solution (3.20). This combination method allows us
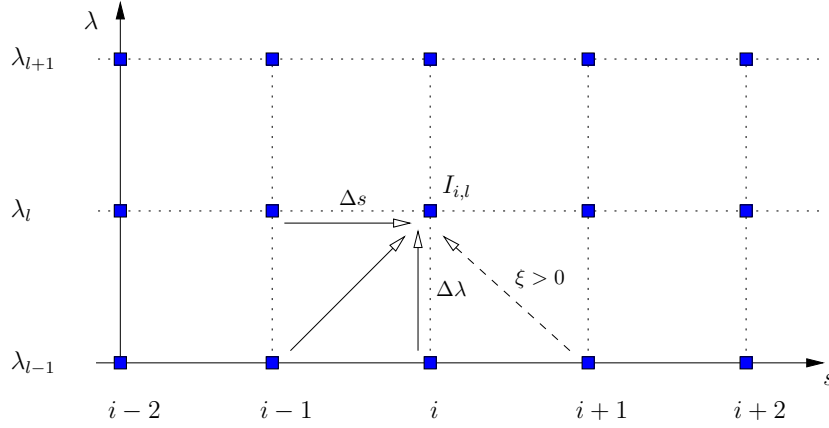
Figure 3.4: The discrete spatial and wavelength grid; the actual intensity $I_{i,l}$ depends on the actual and previous points of the characteristics of the actual and previous wavelength points. The contribution from $I_{i+1,l-1}$ is only needed for a mix with the first discretization method.

to combine and implement both discretization schemes easily and dynamically and to find the optimal combination of stability and accuracy by varying over ξ (Figure 3.4).

3.5   The Line Element in the Comoving Frame

Equations (3.2) and (3.3) form a system of two coupled differential equations. They describe, how the direction of propagation of a photon changes during the transformation from the Eulerian frame into a comoving frame. In the static case $(\beta = 0)$, we get exactly the directional derivatives from (2.24) and (2.25) which describe a constant and straight direction of propagation. As the essential information of (3.2) and (3.3) is how $\vec{n}$ transforms, we do not have to solve them to get the comoving frame angle cosine. From (2.34) we already know, how the angle transforms, and we can use it to calculate the a_λ coefficient.

We emphasized that r and μ are measured in the Eulerian frame, because this is the only inertial frame in which the atmosphere can be described as a whole. As we already mentioned, the line element ds and the finite line element Δs must be measured in the comoving frame. To emphasize the difference to a static atmosphere, we explicitly note the cmf line element as ds' in order to show how we transform the Eulerian frame line element ds. We can make the relations between the Eulerian and comoving frame line elements clear by rewriting the definitions in (3.2) and (3.3) as

$$a_r \partial s' = n_r \partial s$$

$$a_\mu \partial s' = n_\theta \partial s$$

As mentioned above, solving the coupled differential equations (3.2) and (3.3) is not necessary, because we already know how the angle cosine transforms. Instead we reduce the transformation of the line element to a Lorentz transformation of the components of ds.

To do the Lorentz transformations, we rewrite ds as a vector

$$ds' = \begin{pmatrix} dx'_1 \\ dx'_2 \\ dx'_3 \end{pmatrix} \tag{3.21}$$

and describe the relations between the cmf coordinates dx'_i and the Eulerian coordinates dx_j by

$$dx'_i = \frac{\partial x'_i}{\partial x_1}dx_1 + \frac{\partial x'_i}{\partial x_2}dx_2 + \frac{\partial x'_i}{\partial x_3}dx_3 \tag{3.22}$$

The partial derivatives $\frac{\partial x'_i}{\partial x_j}$ are given by the Lorentz matrix in (2.29). As described in section 2.4, equations (3.21) and (3.22) are only valid for the transformation between two inertial frames. But in fact, the comoving frame characteristic passes an infinite number of tangential inertial systems. Hence, the velocity β which determines the Lorentz transformation is not constant. Due to that, we have to integrate over the Lorentz transformations to get the finite element $\Delta x'_i$.

In fact, we want to desribe the physics of the atmosphere in spherical coordinates, but the direction propagation of a characteristic is described in Cartesian coordinates to simplify the vector calculations. Therefore, we switch to Cartesian coordinates and write the transformations of the line element's components as

$$\Delta x' = \int_{x_1}^{x_2}(1 + (\gamma - 1)\frac{\beta_x^2}{\beta^2})dx + \int_{y_1}^{y_2}(\gamma - 1)\frac{\beta_x\beta_y}{\beta^2}dy + \int_{z_1}^{z_2}(\gamma - 1)\frac{\beta_x\beta_z}{\beta^2}dz$$

$$\Delta y' = \int_{x_1}^{x_2}(\gamma - 1)\frac{\beta_y\beta_x}{\beta^2}dx + \int_{y_1}^{y_2}(1 + (\gamma - 1)\frac{\beta_y^2}{\beta^2})dy + \int_{z_1}^{z_2}(\gamma - 1)\frac{\beta_y\beta_z}{\beta^2}dz$$

$$\Delta z' = \int_{x_1}^{x_2}(\gamma - 1)\frac{\beta_z\beta_x}{\beta^2}dx + \int_{y_1}^{y_2}(\gamma - 1)\frac{\beta_z\beta_y}{\beta^2}dy + \int_{z_1}^{z_2}(1 + (\gamma - 1)\frac{\beta_z^2}{\beta^2})dz$$

where (x_1, y_1, z_1) and (x_2, y_2, z_2) are two adjacent intersection points on the characteristic in the Eulerian frame. Then we obtain the finite cmf line element from

$$\Delta s' = (\Delta x'^2 + \Delta y'^2 + \Delta z'^2)^{1/2} \tag{3.23}$$

The integration of the Lorentz transformations is done numerically by a Gauss-Chebyshev quadrature (A.8). In the case of a constant velocity field, the transformation of the line element can be done by a simple Lorentz contraction.

In fact, during the numerical solution of the recursive formal solution (3.20) we calculate the two adjacent intersection points (x_1, y_1, z_1) and (x_2, y_2, z_2) on the characteristic in the Eulerian frame, and then we can derive the cmf line element from (3.23). With this line element, we compute the cmf optical depth.

3.6 The Accelerated Λ-Iteration

In the last section, we presented the numerical monochromatic formal solution (3.20) for the SSRTE (3.4). The sum of all formal solutions for all characteristics on the wavelength and angular

grid gives us the radiation field. Because according to (3.8), the source function determines the mean intensity, we rewrite the formal solution (3.6) formally with the Λ-operator from e.g. [Olson and Kunasz 1987]

$$J_\lambda = \Lambda_\lambda[S_\lambda] \tag{3.24}$$

The problem is that the mean intensities J_ν of the radiation field determine the source function according to (see section 2.2.3)

$$S_\lambda = (1 - \epsilon)J_\lambda + \epsilon B_\lambda \tag{3.25}$$

which has to be consistent with the source function in the formal solution (3.6) and (3.24). While deriving (3.20), we ignored the dependency of the source function on the specific intensities. That is why we call it a *formal* solution. But the RTE in general is an integro-differential equation, as the source function depends on the mean intensity (section 2.3).

To solve this problem, we have to find consistent solutions of the source function and the mean intensities. This is done by a fixed-point iteration scheme called Λ-*iteration*. It is formally written as [Hauschildt 1992]

$$J_\lambda^{\text{new}} = \Lambda_\lambda[S_\lambda^{\text{old}}], \qquad S_\lambda^{\text{new}} = (1 - \epsilon)J_\lambda^{\text{new}} + \epsilon B_\lambda \tag{3.26}$$

But in situations with large optical depths and a small thermal coupling parameter ϵ, the Λ-iteration does not converge fast enough. That is, because the convergence rate of a fixed-point problem is determined by the spectral radius of the iteration matrix. The spectral radius is given by the largest eigenvalue of the iteration matrix. The largest eigenvalue of the Λ-matrix is given by $\lambda_{max} \approx (1 - \epsilon)(1 - T)^{-1}$ where T is the total optical thickness of the medium. Where scattering processes become important and hence, the thermal coupling parameter ϵ is small, the eigenvalue is close to unity in an optically thick medium. The convergence rate of the Λ-iteration then becomes very poor [Mihalas 1980].

We can improve the convergence rate dramatically by splitting the iteration matrix and using parts of the actual solution in the actual iteration step. By introducing the approximate Λ_λ-operator, Λ_λ^*, we split the Λ_λ-matrix according to

$$\Lambda_\lambda = \Lambda_\lambda^* + (\Lambda_\lambda - \Lambda_\lambda^*) \tag{3.27}$$

We rewrite the iteration scheme from (3.26) with the Λ_λ^*-operator by using partly the unknown actual solution of the source function

$$J_\lambda^{\text{new}} = \Lambda_\lambda^*[S_\lambda^{\text{new}}] + (\Lambda_\lambda - \Lambda_\lambda^*)[S_\lambda^{\text{old}}] \tag{3.28}$$

Formally, this is inaccurate, because (3.28) is not consistent with the formal solution from (3.26). But when the iteration has converged and $S_\lambda^{\text{new}} = S_\lambda^{\text{old}}$, this inaccuracy is removed.
By using the source function from (3.26), the iteration scheme becomes

$$J_\lambda^{\text{new}} = \Lambda_\lambda^*\big[(1 - \epsilon)J_\lambda^{\text{new}} + \epsilon B_\lambda\big] + \Lambda_\lambda\big[S_\lambda^{\text{old}}\big] - \Lambda_\lambda^*\big[(1 - \epsilon)J_\lambda^{\text{old}} + \epsilon B_\lambda\big]$$

$$\Leftrightarrow J_\lambda^{\text{new}} = \big[1 - (1 - \epsilon)\Lambda_\lambda^*\big]^{-1}\Big(J_\lambda^{\text{FS}} - (1 - \epsilon)\Lambda_\lambda^*\big[J_\lambda^{\text{old}}\big]\Big) \tag{3.29}$$

$$\Leftrightarrow J_\lambda^{\text{new}} - J_\lambda^{\text{old}} = \big[1 - (1 - \epsilon)\Lambda_\lambda^*\big]^{-1}\big[J_\lambda^{\text{FS}} - J_\lambda^{\text{old}}\big] \tag{3.30}$$

where $J_\lambda^{\mathsf{FS}} = \Lambda_\lambda \big[S_\lambda^{\mathsf{old}} \big]$ is given by the recursive formal solution from (3.20). From (3.30) we notice that the correction $\big[J_\lambda^{\mathsf{FS}} - J_\lambda^{\mathsf{old}} \big]$ between two iteration steps of the ordinary Λ-iteration is now modified by an amplification matrix. That is why equation (3.29) is called *accelerated Λ-iteration* (ALI).

3.6.1   The Construction of the Approximated Λ-Operator

The splitting of the Λ-operator in (3.27) does not invoke any restrictions to the choice of the Λ^*-operator. But to improve the convergence rate significantly compared to the ordinary Λ-iteration, we have to construct the Λ^*-operator in such a way that the eigenvalues of the amplification matrix become very small.
It was shown in [Olson *et al.* 1986] that choosing entries from the original Λ-operator results in optimal convergence rates. Therefore, to use $\Lambda^* = \Lambda$ would be the best choice with respect to the convergence rate. But the construction of the whole Λ-matrix is very time consuming. Furthermore, a more simple structure of the Λ^*-operator makes the solution of the linear system in (3.29) easier and faster. Equation (3.29) can be solved directly by inverting the amplification matrix, but for a complex Λ^*, the matrix inversion becomes very time consuming. By choosing only the diagonal elements of the full Λ-operator, the inversion of the amplification matrix in (3.29) is reduced to a scalar division, but this would not increase the convergence rate very much [Hauschildt 1992].

A good compromise between increasing the convergence rate and the complexity of solving (3.29) is to choose the tridiagonal Λ^*-operator from [Olson and Kunasz 1987] which is constructed from the tridiagonal elements of the original Λ-matrix. A tridiagonal Λ^* improves the convergence rate and can be constructed quickly. Though the solution of equation (3.29) then becomes more complicated than with a diagonal Λ^*-operator, the whole solution process of the RTE is accelerated.

The Λ-operator (3.24) is a formal notation for the formal solution of the SSRTE (2.49). The SSRTE can be solved by the method of characteristics if we assume a known source function S_λ. Therefore, the voxel grid has to be sampled by numerous characteristics of different directions along which the recursive formal solutions (3.20) are computed. The intensities from the solutions of all characteristics are then averaged to get the mean intensity J_λ. The Λ-operator represents this process and is constructed the exact same way.

In the case of a spherical symmetric atmosphere which is discretized by l layers, the source function and the mean intensity become vectors with l entries, one for each layer. In this case, the Λ-operator can be written explicitly as a matrix Λ_{ij}. The jth column of the Λ-matrix is then constructed by assuming a test source function which is zero everywhere except the jth entry and performing a formal solution (see (5.35) from [Knop 2007])

$$\begin{pmatrix} \Lambda_{1j} \\ \Lambda_{2j} \\ \vdots \\ \Lambda_{jj} \\ \vdots \\ \vdots \\ \Lambda_{lj} \end{pmatrix} = \Lambda \cdot \begin{pmatrix} 0 \\ \vdots \\ 0 \\ 1 \\ 0 \\ \vdots \\ 0 \end{pmatrix} \leftarrow j \qquad (3.31)$$

The jth entry from the source function which not equals zero, is called a *pulse*. From (3.31) we notice that an entry $\Lambda_{i,j}$ from the Λ-matrix describes the explicit influence of the source function from layer j on the mean intensity from layer i.

In the case of 3D radiative transfer, the Λ-operator can not be described as a matrix, because it becomes six dimensional. Three dimensions (r, Θ, Φ) are needed to describe a point in the atmosphere. Another set of three local indices (l, m, n) is then needed to describe the contributions of the local pulse to the intensities of the adjacent voxels. Hence, we have to construct a local 3D-$\Lambda^{r\Theta\Phi}$-operator for each voxel of the grid. The equivalence to a tridiagonal Λ-matrix in the 1D case is to restrict the entries $\Lambda^{r\Theta\Phi}_{l,m,n}$-operator to $l, m, n \in \{-1, 0, 1\}$. This implies that we only consider the contributions from the 26 adjacent voxels to the Λ-operator of the centered voxel (*nearest-neighbor*, Figure 3.5).
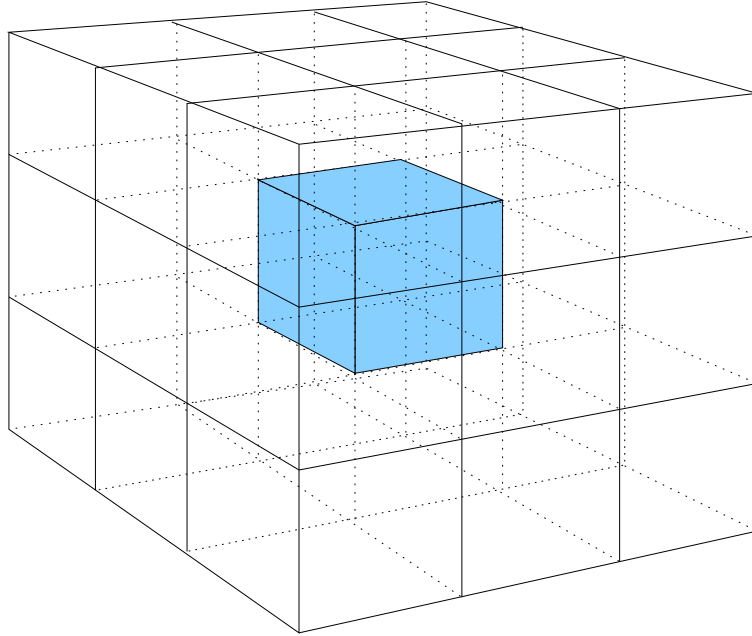

Figure 3.5: A voxel and its 26 neighbors in a Cartesian grid; the nearest-neighbor approach allows the intensity of the centered voxel to influence the source functions of its 26 adjacent neighbors.

However, the principle of the construction of the Λ-elements is the same as described above in the 1D case because the formal solution along a characteristic is the same as in the 1D transfer problem. We have to make sure that the mean intensity at each voxel (not only at each layer as in the 1D problem) is sampled by enough characteristics of different directions.

In the 3D transfer problem, the indices $i(k)$ and $j(k)$ label the voxels that are hit along a characteristic k of a specific direction, where j labels the voxel which Λ-operator we want to construct. They have defined relations to the global coordinates in the grid $(r(j), \Theta(j), \Phi(j))$ and the local indices $(l(i), m(i), n(i))$ of the $\Lambda^{r\Theta\Phi}$-operator at the voxel j [1].

---

[1]For two characteristics k and k', the indices i and j in the 3D case label different voxels and contribute to different entries $\Lambda^{r\Theta\Phi}_{l,m,n}$. This is an important difference to the Λ-construction in the 1D case, where the the indices

We use the recursive formal solution from (3.20) to explicitly compute the contributions $\lambda_{i(k),j(k)}$ from a pulse in a voxel j on the intensity of another voxel i along the characteristic k. As described above, we restrict the Λ-operator to the nearest-neighbor elements. This is equivalent to only allowing explicit influence of the pulse at the voxel j on the intensity of the same voxel at $i = j$ and the adjacent ones $i = j - 1$ and $i = j + 1$. This situation is shown in Figure 3.6 for a static atmosphere.

The contributions of the characteristic k to the entries $\Lambda_{l,m,n}^{r\Theta\Phi}$ in the tridiagonal local $\Lambda^{r\Theta\Phi}$-operator of the voxel at the intersection point j (where the pulse originates) are then computed along the characteristic as follows

$$\lambda_{i(k),j(k)} = 0 \qquad\qquad i < j - 1$$

$$\lambda_{j(k)-1,j(k)} = (1 - \tilde{\beta}_{j-1}\, p_{j-1,l})^{-1}\, \frac{\chi_{j-1,l}}{\hat{\chi}_{j-1,l}}\, \gamma_{j-1} \qquad\qquad i = j - 1$$

$$\lambda_{j(k),j(k)} = (1 - \tilde{\beta}_j\, p_{j,l})^{-1} \left[\lambda_{j-1,j}\, (\tilde{\alpha}_j\, p_{j-1,l} + \exp(-\Delta\tau_{j-1})) + \frac{\chi_{j,l}}{\hat{\chi}_{j,l}}\, \beta_j \right] \qquad\qquad i = j$$

$$\lambda_{j(k)+1,j(k)} = (1 - \tilde{\beta}_{j+1}\, p_{j+1,l})^{-1} \left[\lambda_{j,j}\, (\tilde{\alpha}_{j+1}\, p_{j,l} + \exp(-\Delta\tau_j)) + \frac{\chi_{j+1,l}}{\hat{\chi}_{j+1,l}}\, \alpha_{j+1} \right] \qquad i = j + 1$$

$$\lambda_{i(k),j(k)} = 0 \qquad\qquad i > j + 1$$

For $i < j - 1$ and $i > j + 1$ the contributions vanish because of the nearest-neighbor structure we chose for the Λ-operator. However, it is possible to compute the full bandwidth of the Λ-operator by allowing the pulse from voxel j to propagate beyond the voxel $i = j + 1$, where it causes exponentially damped contributions to the intensities [Hauschildt and Baron 2004]. In the 3D case, this would cause a cubic growth of n^3 ($n = $ number of allowed adjacent voxels along the characteristic to be influenced) of the Λ-operator and would cause the storage problems discussed above.

Now we are able to build the $\Lambda_{l,m,n}^{r\Theta\Phi}$-elements. The intersection points i of the voxels along a characteristic have to be transformed into the local coordinates $(l(i), m(i), n(i))$ of the $\Lambda^{r\Theta\Phi}$-operator at the voxel $(r(j), \Theta(j), \Phi(j))$. If we sample the atmosphere with an appropriate number of characteristics from different directions for each voxel, we then finally get the tridiagonal $\Lambda_{l,m,n}^{r\Theta\Phi}$-elements by summing the contributions $\lambda_{i(k),j(k)}$ from all characteristics

$$\Lambda_{l(i),m(i),n(i)}^{r(j)\Theta(j)\Phi(j)} = \sum_k w_{i(k),j(k)} \lambda_{i(k),j(k)} \qquad\qquad (3.32)$$

where the $w_{i,j}$ are the angular quadrature weights. The coordinate transformations are not done analytically because they are a result of the numerical approach to build the Λ-operator by the method of characteristics. Therefore, they are done stepwise during the formal solution along a characteristic.

---

of different characteristics must always label the same layer and therefore contribute to the same entries $\Lambda_{i,j}$.
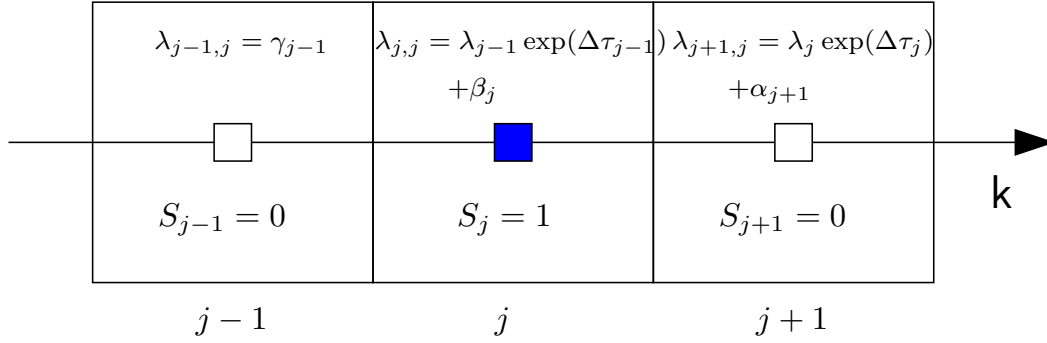
Figure 3.6: The characteristic k passes the adjacent voxels $j-1$, j and $j+1$; the construction of the $\lambda_{i,j}$-contributions is done by a recursive formal solution along the characteristic. The test source term in the centered voxel j contains the pulse which then determines the intensity of the adjacent voxels because of the parabolic interpolation the formal solutions is based on (compare to (3.7) and (3.8)). For simplification, the situation in this figure assumes a static atmosphere and a cubic voxel grid. In fact, we use a spherical grid (Figure 3.3), and in the presence of a velocity field, the $\lambda_{i,j}$-contributions have to be adjusted by the wavelength-dependent terms according to the cmf recursive formal solution (3.20).

3.7   The Affine Method

The method from [Mihalas 1980], we described above, is based on an RTE that describes radiative transfer in a comoving frame. Actually, this comoving frame is a mixed frame, because the spatial coordinates are measured in the observer's frame and the two momentum variables μ and λ in the comoving frame. By this, we use the advantages of describing the physics of the moving matter in its rest frame. But the mixing of observer's spatial coordinates and comoving momentum variables causes an apparent curvature of the characteristics (described by (3.2) and (3.3)) which is in fact not observable.

The curvature of the characteristics can be avoided by only measuring the wavelength in the comoving frame which is transformed easily according to (2.32). This ansatz is described in detail in [Chen *et al.* 2007] and leads to an RTE of the form

$$\left.\frac{\partial I_\lambda}{\partial s}\right|_\lambda + a(s)\frac{\partial I_\lambda}{\partial \lambda} = -[\chi_\lambda f(s) + 5a(s)]I_\lambda + \eta_\lambda f(s) \tag{3.33}$$

which is written in terms of an *affine* parameter ξ. The parameter s measures the distance in the observer's frame and is related to the affine parameter by

$$s = \frac{h}{\lambda_\infty}\xi \tag{3.34}$$

where λ_∞ is the observer's frame wavelength.

We use this method to compare and verify our results, as the affine method is already implemented in the 3D framework of PHOENIX [Baron *et al.* 2009].

Chapter 4

Implementation and Tests

In this chapter we describe the implementation process of the solution methods described in the previous chapter. We describe the tests we did to verify the implementation, and we discuss computational aspects that are important for 3D radiative transfer.

4.1 Introduction

The implementation of the 3D solution scheme presented in the last chapter, also called *solver*, has to be tested extensively before it can be applied to the problems of stellar atmospheres. During the implementation process, we did several consistency tests in order to minimize the number of error sources. First of all, we had to assure the inner consistency of the formal solution and the Λ^* construction. As described in section 3.6, the nearest-neighbor Λ^*-operator for a certain voxel is constructed by assuming a pulse in that voxel and computing a formal solution. Therefore, we tested the inner consistence of the solver by computing a formal solution for a grid in which the source function of only one voxel is set to unity and zero everywhere else. Then the formal solution of that voxel and its 26 nearest-neighbors and the 27 entries of the Λ^*-operator of the centered voxel have to be identical. Furthermore, the recursive formal solution (3.20) which includes the effects of a velocity field, has to reproduce the results of the static formal solution (3.7) if $v(r)$ equals zero for all r. Verifying this consistency was also very helpful during the implementation process. Finally, we could test the wavelength coupling for the case of a hypothetic two-level atom (see section 2.5). The solution scheme presented in chapter 3 has already been implemented successfully in the 1D framework of PHOENIX [Hauschildt and Baron 2004] and acted as reference for a reasonable solution of our implementation in the 3D framework.

4.2 The Solution Scheme - An Overview

The solution scheme, we presented in chapter 3, consists of the following basic steps

a) the computation of a formal solution J_{FS} or $\bar{J}_{\mathsf{FS}}$

b) the construction of the Λ^*-operator

c) the solution of equation (3.29) which gives J_{new} or $\bar{J}_{\mathsf{new}}$

d) the accelerated Λ-iteration

Hence, these steps determine the time needed to find a consistent solution of the RTE. In the case of 3D radiative transfer, the time to solve the RTE is scaled dramatically because of the increase in spatial *and* solid angle dimensions. This makes *parallelization* indispensable in the 3D case.

In Figure 4.1 the pseudo code of the 3D solver is shown. The processes in the dashed-outlined box can be parallelized because the method of characteristics allows us to compute formal solutions for different directions independently. By this, we can simply reduce the time to solve the 3D RTE by scaling up the number of *central processing units* (cpu). Each cpu gets a *task* to compute the formal solution of certain solid angles only.
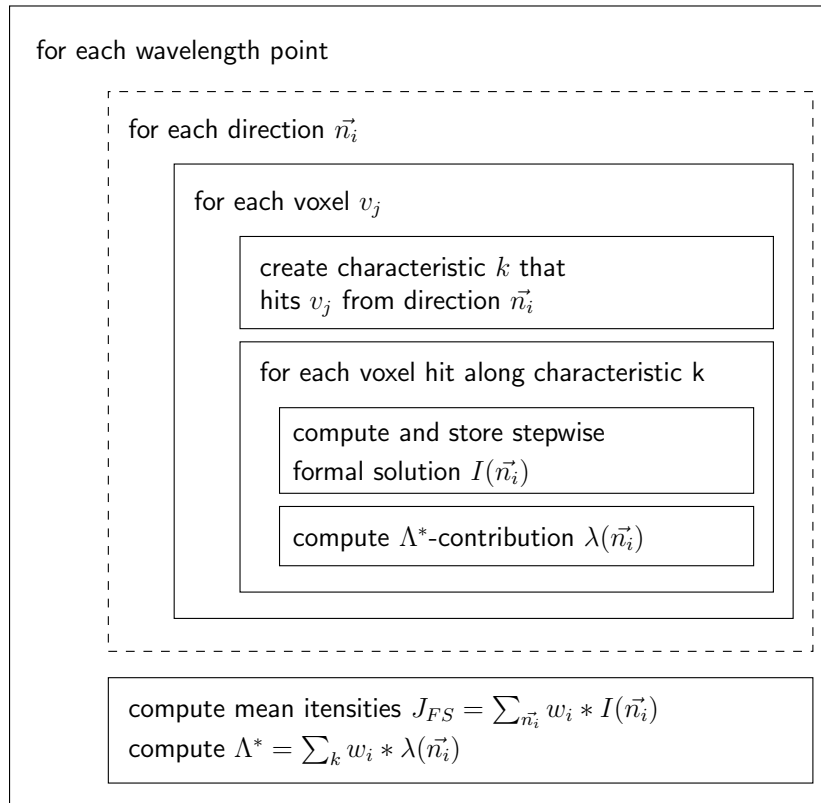

Figure 4.1: The pseudo code for the solver; the formal solution process for a certain wavelength point is shown. The processes in the dashed-outlined box can be parallelized, because the formal solution for a certain direction does not contain contributions from any other directions.

4.3 An Estimation of Memory Requirements

From the recursive formal solution (3.20) and Figure (3.4) we noticed that we need to know the specific intensities I_{l-1} for all characteristics from the previous point on the wavelength grid in order to be able to calculate the actual solution step. This coupling is a special relativistic effect due to the velocity field. For the numerical solution of the RTE, we have to store these intensities. But in the 3D case, we have to store the specific intensities for each voxel in the spatial grid and for each solid angle $\vec{n}$ individually.

As we will see in the following section 4.4, the number of solid angles is essential for the accuracy

of the 3D-RTE solution. But the angular resolution also scales the memory that is required for the storage of the specific intensities dramatically.

In the following, we denote the number of angular points for ϕ and θ by n_ϕ and n_θ. The memory requirement of the specific intensities I_{l-1} is then scaled by a factor of $(n_\phi * n_\theta)$ in comparison to all other physical quantities that have to be stored for a certain voxel.

For an example, we assume that we need a resolution of 128 angular points for ϕ and θ which is a typical resolution we used for testing purposes. This means that the memory requirement for the specific intensities is scaled by a factor of $128^2 = 16.384$. As we want to use a double precision accuracy (8 byte) during the computations, we can estimate the memory required for a 3D grid of a spatial resolution of $(128 * 64 * 128)$ voxels by

$$(128 * 64 * 128) \,\text{voxel} * 128^2 \,\text{angle/voxel} * 8 \,\text{byte/angle} \approx 137 \text{GB}$$

Hence we need 137 GB of memory to store the specific intensities I_{l-1} for the whole grid in this exemplary case. This becomes a problem as we have to store the grid data in the *random-access memory* (RAM) for fast data transfer. Therefore, we could either parallelize the computation on a *shared memory* system where several cpu's share the same RAM, or we could also parallelize the memory management. The latter uses the fact that a single cpu with its own RAM only needs to store the specific intensities of the solid angles its task contains. When the computations are finished, the grid data has to be exchanged between the cpu's. This process is called *data reduction*. Although the data reduction process slows the overall computation processes down, the parallelization of memory management makes the scaling processes more dynamic when we want to increase the grid resolution or the number of solid angles. If the resolutions exceed the example above, as we will see is necessary, the memory required to store the specific intensities I_{l-1} easily increases to terabytes or beyond.

4.4   Tests

For the following tests we devised a simple test model of a two-level atom with background continuum to test the wavelength coupling in the formal solution (see section 2.5.2). The model distinguishes between continuum and line opacities $\chi_c = \epsilon_c \kappa_c + (1-\epsilon_c)\sigma_c$ and $\chi_l = \epsilon_l \kappa_l + (1-\epsilon_l)\sigma_l$. The line of the two-level atom is parameterized by its relative strength to the continuum opacity χ_l/χ_c and its thermalization probability $\epsilon_l = \kappa_l/\chi_l$. For the intrinsic line profile ϕ_l we use a Gaussian profile which is discretized dynamically by 56 points on the wavelength grid.

For the spatial discretization of the test atmosphere we use a spherical 3D grid. The resolution of the grid is defined by

- n_r - number of radial grid points or *layers*

- n_Θ - number of grid points in the Θ coordinate

- n_Φ - number of grid points in Φ

The grid consists of a number of $(n_r * n_\Phi * n_\Theta)$ voxels. The resolution on the solid angle grid is determined by

- n_θ - number of angular points in θ

- n_ϕ - number of angular points in ϕ

The extension of the test atmosphere is $10 * 10^6 km$ with an inner radius at $R_{in} = 0.1 * 10^6 km$ and the outer radius at $R_{out} = 10.1 * 10^6 km$. The optical depth ranges on a logarithmic scale from $\tau_{in} = 10^4$ to $\tau_{out} = 10^{-4}$ in the continuum. The velocity field is linearly increasing with a prescribed maximum velocity $\beta(R_{out}) = \beta_{max}$.

The total number of solid angles per voxel is given by $(n_\theta * n_\phi)$. It is crucial for the 3D solution to choose an appropriate number of solid angles, as it determines the accuracy of the angular integration. For the test calculations, we chose at least $n_\theta = n_\phi = 32$ so that we get a minimum of 1024 solid angles.

In all of the following tests, we used a grid containing a spherically symmetric structure so that we can compare the results directly to 1D solutions. Because of the spherical symmetry, the number of layers (n_r) in the voxel grid is also crucial for the accuracy of the 3D-RTE solution. We chose at least $n_r = 64$ layers.

4.4.1 The Transformation of the Line Element

The transformation of the line element ds is a crucial part in calculating the cmf opacity (see section 3.5). The following test was done to verify the transformation of the line element ds from section 3.5. In order to compare the line elements ds and ds' of the Eulerian and Lagrangian frame, we choose a radial characteristic and compare the spatial steps ds that are done during the stepwise formal solutions along the characteristic with the results from equation (3.23).

In Figure 4.1 the quotient of ds' and ds is compared with the Lorentz factor $\gamma = (1 - \beta^2)^{-1/2}$. It is obvious that the result is almost identical with a Lorentz contraction

$$ds' = \gamma ds \qquad (4.1)$$

Figure 4.2 shows the differences in detail. The quadrature solution 3.5 differs from (4.1) in the case of relativistic velocities larger than $\frac{c}{2}$ with a maximum of 5%. The consistency originates from the homology nature and the constant gradient of the velocity field (compare to 2.27). Although the velocity field is restricted to a monotonic form, we must not approximate the cmf line element with a Lorentz contraction in general because the velocity field may contain regions of larger (smaller) gradients (e.g. supernovae). Nevertheless, the constant gradient allows us to verify our results for the cmf line element as the Lorentz factor γ gives us a good indication for a reasonable solution.

4.4.2 Continuum Tests

As a first test, we computed a purely absorptive continuum solution ($\epsilon_c = 1$) for different maximum velocities β_{max} because this should be reproduced by the algorithm. We tested the continuum solution for a grid with a resolution of $n_r = n_\Phi = 2 * 32 + 1$ and $n_\Theta = 2 * 16 + 1$ points along each axis. For the angular resolution we used $n_\theta = n_\phi = 64$ points for a total of 4096 solid angles. From Figure 4.3 we notice that the solutions for the discretization methods $\xi = 1$ and $\xi = 0$ are identical for a zero expansion velocity and reproduce the flat continuum. The solutions are also nearly identical for increasing β_{max}. For a maximum velocity of $\beta_{max} = 0.1$, we notice a slight variation in the continuum for both discretization methods. This is caused by the initial conditions on the wavelength grid. Once they are "forgotten", the flat continuum is reproduced. Figure 4.3 also shows that the 3D continuum solution has a certain bandwidth in J. This is because we plotted the cmf J for every voxel at the surface of the spherical voxel grid. Due to the
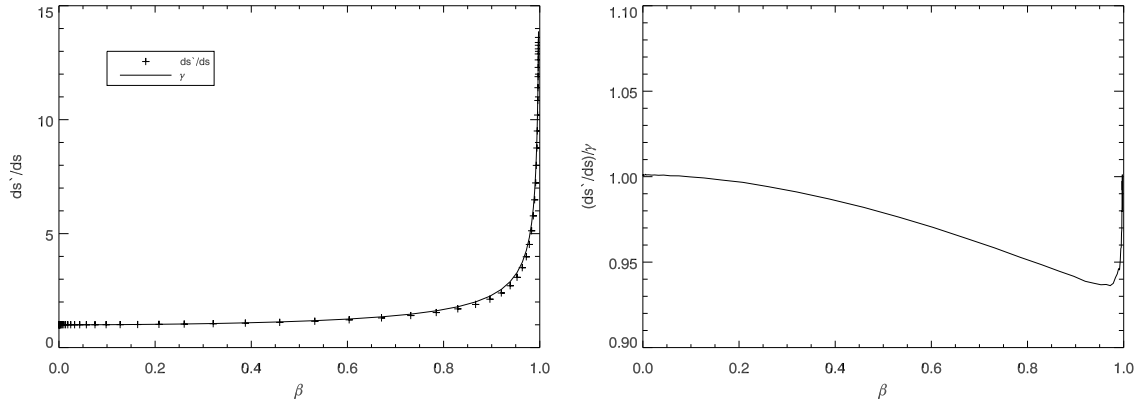
Figure 4.2: Test of the line element transformation for a radial characteristic using 64 layers; the ratio of ds' and ds is compared to the Lorentz factor γ. The velocity gradient influences the solution only for large relativistic velocities with a maximum of 5% compared to the Lorentz factor. Near $\beta=1$, both (ds'/ds) and γ become infinite.

limited angular and spatial resolution, J is not totally consistent at the surface. The consistency of the surface solution depends strongly on the number of solid angles as we will show in the following section.

4.4.3   NLTE Line Tests

For the line transition tests, the background continuum is assumed to be purely absorptive ($\epsilon_c = 0$). We set the line strength $\chi_l/\chi_c = 100$ to simulate a strong scattering dominated line with $\epsilon_l = 0$. Again, we used a grid with a resolution of $n_r = n_\Phi = 2*32+1$ and $n_\Theta = 2*16+1$ points. We varied the number of solid angles to determine the influence on the consistency of the surface J. For the line transition calculations, the accelerated Λ-iteration is applied to $\bar{J}$ and converged after 22 iterations. The computation for $64*64 = 4096$ solid angles took 48 hours on the "Seneca"-cluster at the Hamburger Sternwarte using 36 AMD Opteron 1.8 MHz processors. The results for $\beta_{max} = 0.0, 0.01$ and 0.1 and different angular resolutions are shown in Figure 4.4. As in the continuum tests, the static solutions are reproduced successfully for $\beta_{max} = 0.0$. With increasing velocities, we notice a red-shift in the lines shapes due to the velocity field. It is obvious that a larger number of solid angles significantly improves the accuracy of the mean intensities, when we compare the solutions for different numbers of solid angles. At the same time, we reach a limit for reasonable computation times needed for testing purposes with 64^2 solid angles on 36 processors. This emphasizes the need for large scale computer clusters in order to get accurate results.

In Figure 4.5, we compare the results of 3D calculations with the 1D solutions for different maximum velocities. The line shape of the 3D results show excellent agreement with the 1D calculations. But with increasing velocities, both the background continuum and the line of the 3D solutions show an offset downwards of about 5% for $\beta_{max} = 0.05$ and 12% for $\beta_{max} = 0.1$. This may be an effect of our limited angular resolution. The comparison of the results from Figure 4.4 and 4.5 also shows no difference between the two discretization methods. Nevertheless, the numerical instabilities for the $\xi = 0$ discretization described in [Hauschildt and Baron 2004] may also appear in the 3D case and have to be investigated in further spectral computations.
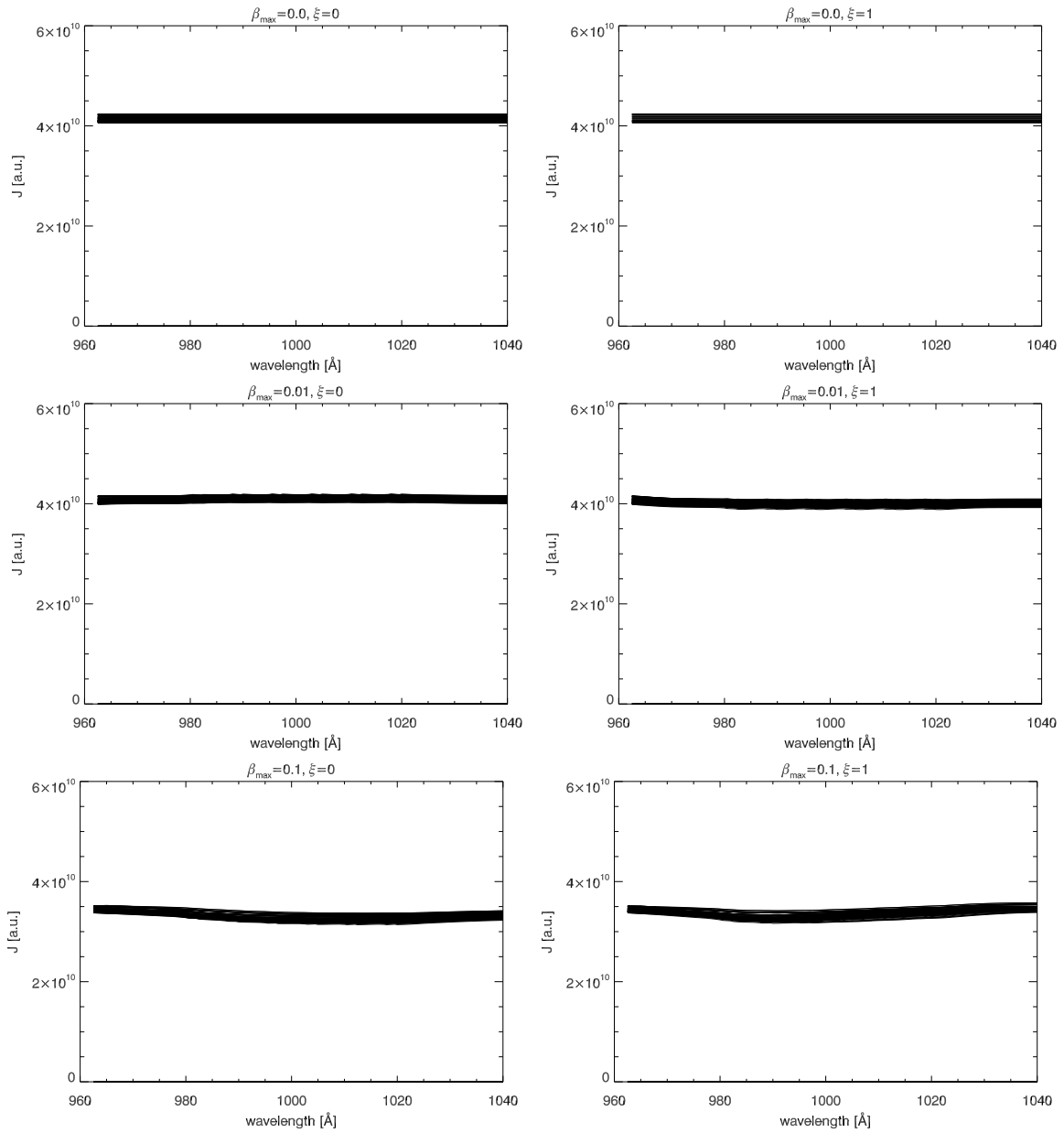
Figure 4.3: The absorptive continuum; *left part:* discretization $\xi=0$, *right part:* discretization $\xi=1$; the static continuum solution is reproduced successfully for $\beta_{max} = 0$. The solutions for increasing velocities show slight variations in the continuum due to the initial conditions on the wavelength grid. J is plotted in arbitrary units (a.u.), as we are not interested in absolute values.
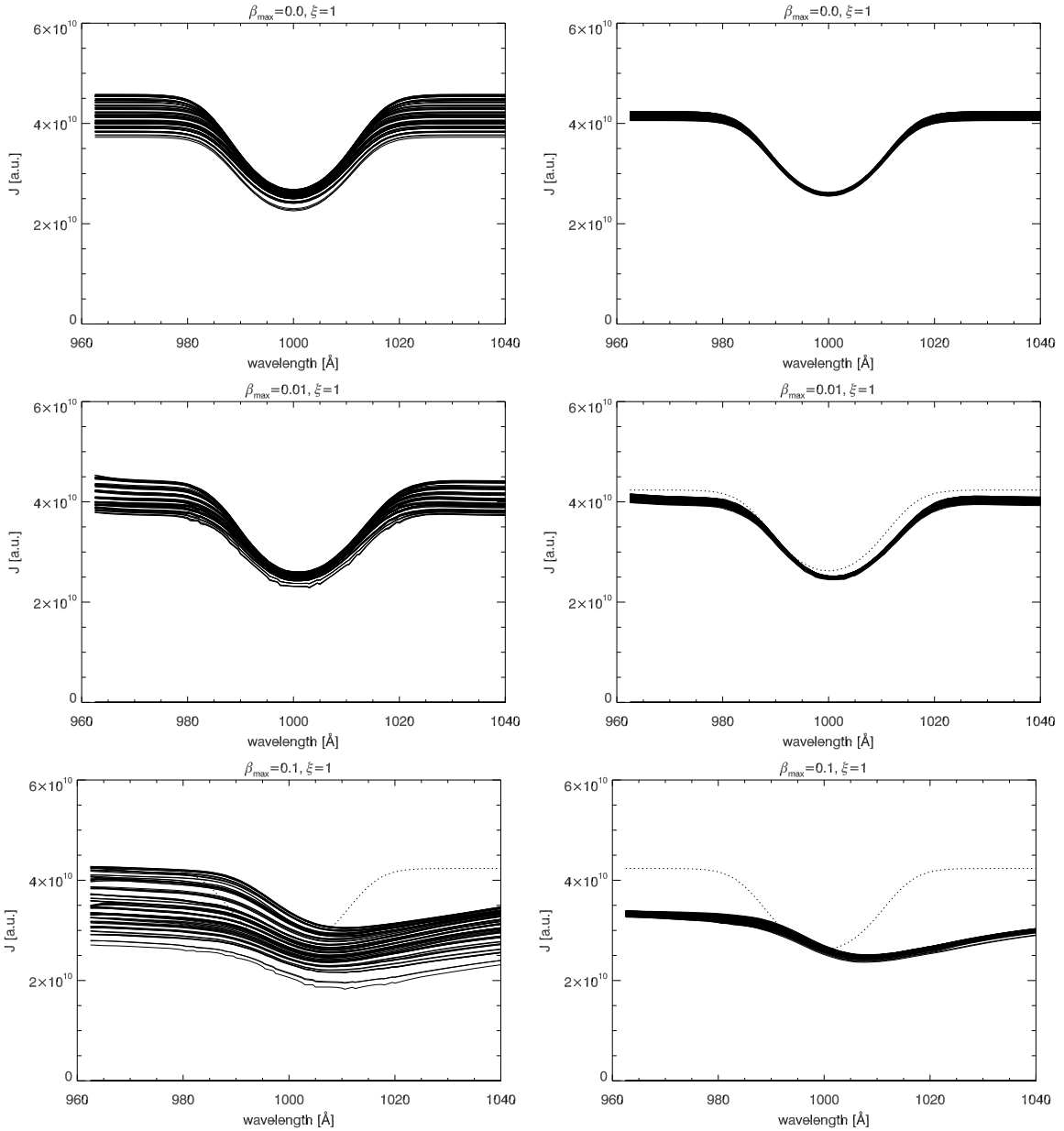
Figure 4.4: NLTE line transitions for different angular resolutions and maximum velocities for $\xi = 1$; *left part:* the results for $\beta_{max} = 0.0$ and 0.01 and $n_\theta = n_\phi = 16$ and $\beta_{max} = 0.1$ and $n_\theta = n_\phi = 8$; *right part:* the results for $\beta_{max} = (0.0, 0.01, 0.1)$ and $n_\theta = n_\phi = 64$; the dotted line indicates the original line shape for a static solution which is successfully reproduced by the solver for $\beta_{max} = 0.0$. For an increasing β_{max} we notice how the line is red shifted due to the effects of the velocity field. The number of solid angles is crucial for the bandwidth and accuracy of the surface J solution.
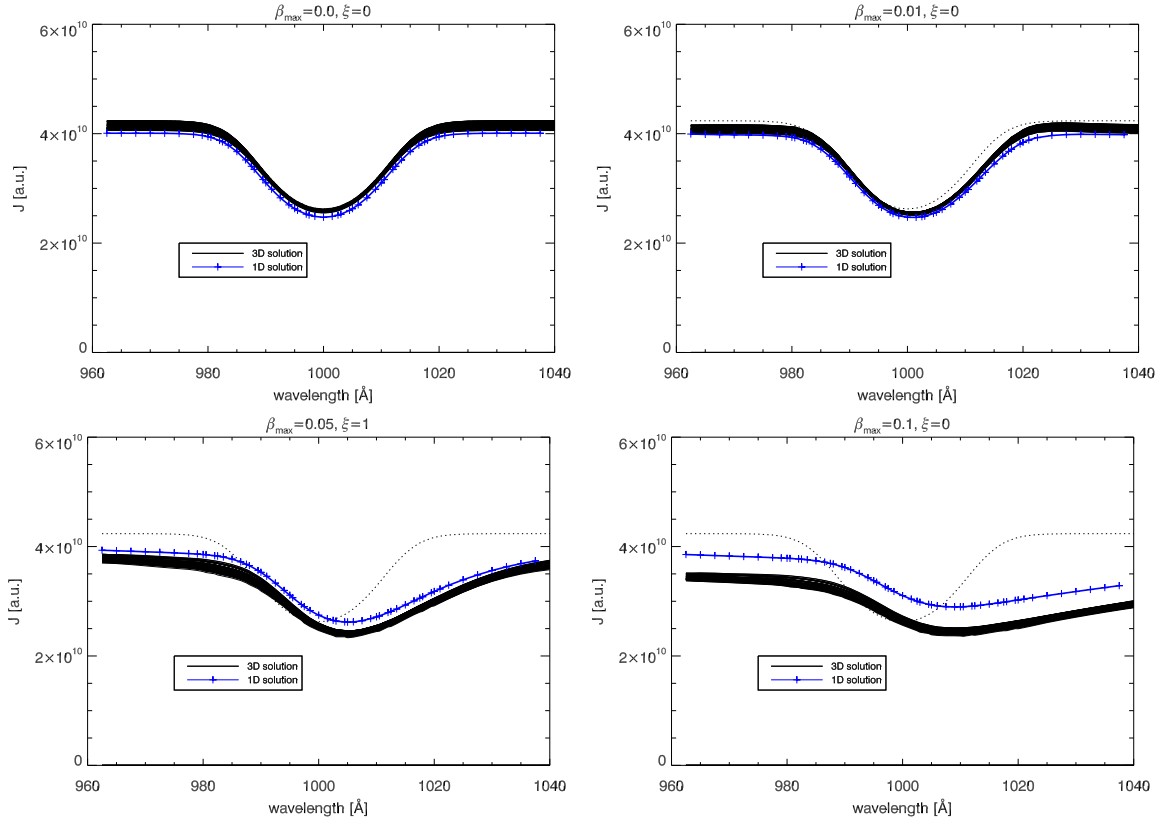
Figure 4.5: The results of 3D calculations for different scattering lines are compared with 1D-calculations for the maximum velocities $\beta_{max} = (0.0, 0.01, 0.05, 0.1)$; the dotted line indicates the original line shape for a static solution. We used $n_\phi * n_\theta = 64^2$ solid angles and 64 layers for discretization.

To verify the offset between the 1D and the 3D solutions, we compare the results of the *grey* solution. That means, we solve the RTE for the monochromatic source function from (2.10). We can then increase the spatial and angular resolutions to improve the accuracy of the 3D solution since we do not have to solve the RTE along the wavelength grid. Furthermore, we assume an LTE situation with $\epsilon = 1$ so that the iteration converges after the second step. By this, we were able to increase the angular resolution to a maximum of $n_\phi * n_\theta = 128^2 = 16384$ solid angles with 128 layers.

In Figure 4.6, we compare the solutions of J as a function of distance from the center. In addition to the 1D and 3D calculations, the results of the affine method described in section 3.7 are shown. Our extended Mihalas method turns out to be extremely dependent on a large number of solid angles as it deviates from the 1D solution in the outer layers where the velocity is at maximum. This may be an effect of the extreme curvature of the characteristics in the Mihalas comoving frame. The curvature for relativistic velocities would then distort our observers frame number of solid angles. With the power of local computation clusters with up to 48 AMD Opteron processors, we were not able to increase the number of solid angles to get an accurate 3D solution in a reasonable time that reproduces the 1D calculation exactly.

Since for the line tests we plot the mean intensities of the surface voxels, an inaccurate angular solution in the regions of maximum velocity would then cause the offset in the line calculations. The affine method reproduces the 1D solution very well, because the angular integration is done

in the affine comoving frame, where the number of solid angles stays accurate. The slight offset of both our 3D Mihalas and the affine method in comparison to the 1D solution even in the inner layers is also an effect of the limited angular resolution. As shown in [Baron *et al.* 2009], the affine method reproduces the 1D Mihalas solution very well for a number of at least 256^2 solid angles. Computations in [Baron *et al.* 2009] were done by using up to $2^{14} = 16.384$ processors on the Franklin Cray XT4.

However, the shape of the line profiles is reproduced very well by our 3D solver. For the verification of the absolute intensity offset, further computations on large scale computer cluster are required in order to achieve angular resolutions that are comparable to the ones used in [Baron *et al.* 2009].
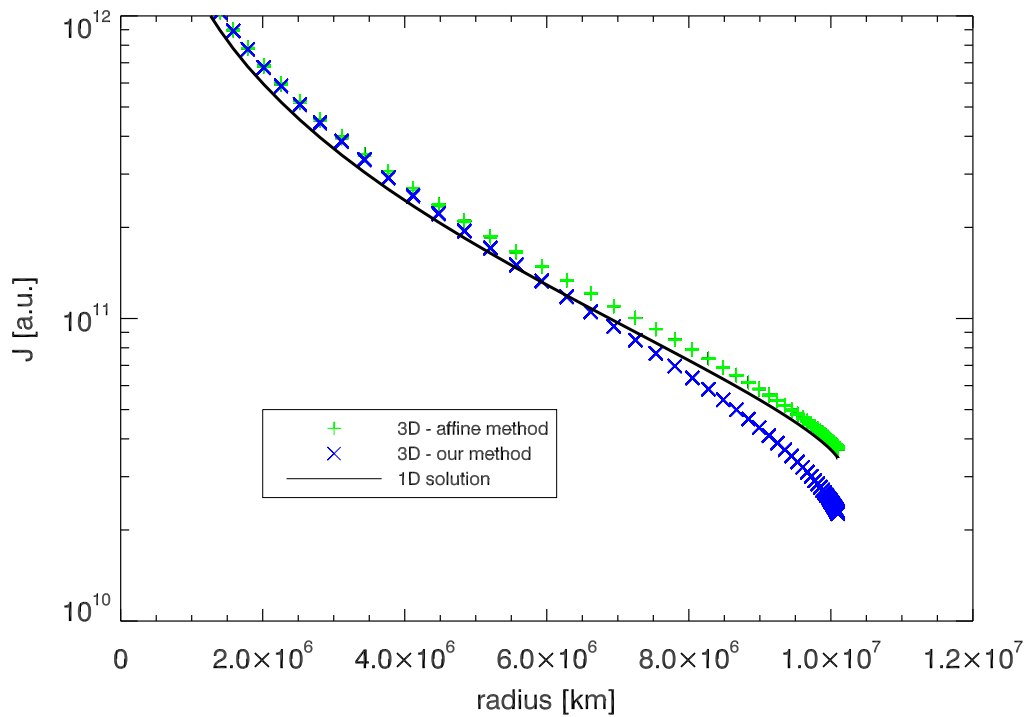

Figure 4.6: The results of the gray 3D-RTE solutions for $\beta_{\max} = 0.33$, $n_\theta * n_\phi = 128^2$ solid angles and 128 layers are compared to the 1D solution.

Chapter 5

Conclusions and Outlook

For the solution of the special relativistic 3D radiative transfer equation, we extended the method described by Mihalas in order to implemented it in the 3D radiative transfer framework of PHOENIX. The intensities are calculated in a comoving frame with the momentum variables μ and λ measured in the comoving frame. Another solver had already been implemented in PHOENIX which is based on the method described in [Chen *et al.* 2007]. This affine method measures only the wavelength in the comoving frame so that the Lorentz transformations along the characteristics are avoided. We have shown that our implementation of the Mihalas approach reproduces the 1D continuum and the shape of line transition calculations for a spherically symmetric test atmosphere. But it also became obvious that the number of solid angles used for the angular integration of the intensity is crucial for the accuracy of the 3D solution. We calculated gray solutions of the RTE with up to 128^2 solid angles, but the Mihalas method still shows offsets in the total mean intensity values. The affine method shows a better consistency with the 1D solution for smaller angular resolutions. This may be a result of the solid angles being calculated in the observers frame so that the curvature of the characteristics is avoided. In the Mihalas comoving frame, the curvature of the characteristics may be the reason for the angular resolution being distorted. This has to be a subject of further investigation of the Mihalas method being used for 3D radiative transfer. Dynamic velocity dependent angular discretization may be desirable.

PHOENIX now contains two 3D and a 1D cmf solver for the calculation of special relativistic radiative transfer with monotonic radial velocity fields. It is always important to solve the RTE by different methods in order to check the consistency of the model. An approach to solve the 3D-SSRTE in the observer's frame has also been implemented recently. The extension of the PHOENIX 3D framework for special and general relativistic radiative transfer with arbitrary velocity fields as described in [Baron and Hauschildt 2004] and [Chen *et al.* 2007] is an actual subject of research. The integration of the 3D radiative transfer framework into the full real world code of PHOENIX and the application to real astrophysical problems will be object of future work.

Appendix A

Gaussian Quadrature

The idea of the Gaussian quadrature, named after Carl Friedrich Gauss, is to approximate an integral by a sum of weighted function values at specified evaluation points inside the integration interval [Press *et al.* 2007]. The integrand function $f(x)$ is separated in a weighting function $w(x)$ and a continuous function $\Phi(x)$ which is approximated by a polynomial

$$f(x) = w(x)\,\Phi(x) \tag{A.1}$$

The integration of $f(x)$ in the intervall $[-1, 1]$ then becomes

$$\int_{-1}^{1} f(x)\,dx = \int_{-1}^{1} w(x)\Phi(x)\,dx \approx \sum_{i=1}^{n} w_i \Phi(x_i) \tag{A.2}$$

The evaluation points x_i are chosen with respect to maximum accuracy. The Gaussian quadrature yields exact results for polynomials of orders up to $(2n-1)$. The optimal evaluation points for an n-point Gaussian quadrature are determined by the roots the polynomials of a class of orthogonal polynomials. The class of orthogonal polynomials is determined by the weighting function $w(x)$.

A.1   Gauss-Chebyshev Quadrature

The Gauss-Chebyshev quadrature is a Gaussian quadrature with the weighting function

$$w(x) = \frac{1}{(1 - x^2)^{1/2}} \tag{A.3}$$

It is used for integrals of the form

$$\int_{-1}^{1} \frac{g(x)}{(1 - x^2)^{1/2}} dx \tag{A.4}$$

For an arbitrary continuous integrand $f(x)$, the Gauss-Chebyshev quadrature can be applied by separating $f(x)$ according to

$$f(x) = w(x)\,(1 - x^2)^{1/2}\,f(x) \tag{A.5}$$

The evaluation points x_i are given by the roots of the Chebyshev polynomials

$$x_i = \cos\left(\frac{2i + 1}{2n + 2}\right), \quad 0 \leq i \leq n \tag{A.6}$$

with the constant weights

$$w_i = \frac{\pi}{(n+1)} \tag{A.7}$$

The integral is then approximated according to A.2

$$\int_{-1}^{1} f(x)\, dx = \int_{-1}^{1} w(x)\,(1-x^2)^{1/2} f(x)\, dx \approx \sum_{i=1}^{n} w_i (1-x_i^2)^{1/2}\, f(x_i) \tag{A.8}$$

A.2 Gaussian Quadrature for an Arbitrary Integration Interval

The Gaussian quadrature can be applied on arbitrary integration intervals over [a,b] by a transformation of the variable

$$t = \frac{a+b}{2} + \frac{a-b}{2}\, x, \quad dt = \frac{b-a}{2}\, dx \tag{A.9}$$

The integral is then transformed into the interval over $[-1, 1]$ by

$$\int_{a}^{b} f(t)\, dt = \frac{b-a}{2} \int_{-1}^{1} f\left(\frac{a+b}{2} + \frac{a-b}{2}\, x\right) dx \tag{A.10}$$

and the Gauss quadrature rule may be applied.

Bibliography

[Baron and Hauschildt 2004] E. Baron and P. H. Hauschildt. Co-moving frame radiative transfer in spherical media with arbitrary velocity fields. *Astronomy & Astrophysics*, 427:987–994, December 2004.

[Baron *et al.* 2009] E. Baron, P. H. Hauschildt, and B. Chen. A 3D radiative transfer framework. V. Homologous flows. *Astronomy & Astrophysics*, 498:987–992, May 2009.

[Castor 1972] J. I. Castor. Radiative Transfer in Spherically Symmetric Flows. *Astrophysical Journal*, 178:779–792, December 1972.

[Chen *et al.* 2007] B. Chen, R. Kantowski, E. Baron, S. Knop, and P. H. Hauschildt. Steps for solving the radiative transfer equation for arbitrary flows in stationary space-times. *Monthly Notices of the Royal Astronomical Society*, 380:104–112, September 2007.

[Gray 1992] D. F. Gray. *The observation and analysis of stellar photospheres*. 1992.

[Hauschildt and Baron 1999] P. H. Hauschildt and E. Baron. Numerical solution of the expanding stellar atmosphere problem. *Journal of Computational and Applied Mathematics*, 109:41–63, September 1999.

[Hauschildt and Baron 2004] P. H. Hauschildt and E. Baron. Improved discretization of the wavelength derivative term in CMF operator splitting numerical radiative transfer. *Astronomy & Astrophysics*, 417:317–324, April 2004.

[Hauschildt and Baron 2006] P. H. Hauschildt and E. Baron. A 3D radiative transfer framework. I. Non-local operator splitting and continuum scattering problems. *Astronomy & Astrophysics*, 451:273–284, May 2006.

[Hauschildt *et al.* 1997] P. H. Hauschildt, E. Baron, and F. Allard. Parallel Implementation of the PHOENIX Generalized Stellar Atmosphere Program. *Astrophysical Journal*, 483:390–+, July 1997.

[Hauschildt 1992] P. H. Hauschildt. A fast operator perturbation method for the solution of the special relativistic equation of radiative transfer in spherical symmetry. *Journal of Quantitative Spectroscopy and Radiative Transfer*, 47:433–453, June 1992.

[Knop *et al.* 2007] S. Knop, P. H. Hauschildt, and E. Baron. General relativistic radiative transfer. *Astronomy & Astrophysics*, 463:315–320, February 2007.

[Knop 2007] S. Knop. General Relativistic Radiative Transfer. *doctoral thesis*, 2007.

[Mihalas 1978] D. Mihalas. *Stellar atmospheres /2nd edition/*. 1978.

[Mihalas 1980] D. Mihalas. Solution of the comoving-frame equation of transfer in spherically symmetric flows. VI - Relativistic flows. *Astrophysical Journal*, 237:574–589, April 1980.

[Olson and Kunasz 1987] G. L. Olson and P. B. Kunasz. Short characteristic solution of the non-LTE transfer problem by operator perturbation. I. The one-dimensional planar slab. *Journal of Quantitative Spectroscopy and Radiative Transfer*, 38:325–336, 1987.

[Olson *et al.* 1986] G. L. Olson, L. H. Auer, and J. R. Buchler. A rapidly convergent iterative solution of the non-LTE radiation transfer problem. *Journal of Quantitative Spectroscopy and Radiative Transfer*, 35:431–442, 1986.

[Press *et al.* 2007] W. H. Press, B. P. Flannery, W. T. Vetterling, and S. A. Teukolsky. *Numerical recipes 3rd edition. The art of scientific computing*. 2007.

[Wang and Wheeler 2008] L. Wang and J. C. Wheeler. Spectropolarimetry of Supernovae. *Annual Review of Astronomy & Astrophysics*, 46:433–474, September 2008.

Acknowledgements

I would like to thank:

Prof. P. H. Hauschildt, for providing me with a very interesting topic in the field of theoretical and computational astrophysics and for the great help and guidance during the work.

Dr. Sebastian Knop, for his great help and infinite patience. I was not able to find a question he could not answer.

Prof. J. Schmitt, for being the second referee on this thesis.

Furthermore, I would like to thank all my colleagues at the Hamburger Sternwarte, especially the members of the PHOENIX group. Special thanks go to my various office mates, for their time, help and support.

Finally, there are people, who not only supported me during the time I spend working on this thesis but also during the last five years of studying and beyond. This includes my family and friends, especially Alewtina, Felix and Maren.

Special thanks go to my parents, who always supported and encouraged me in forging ahead.

Besonderer Dank gebührt meinen Eltern, die mich immer dabei unterstützt und ermutigt haben, meinen Weg zu gehen.

Erklärung

Hiermit versichere ich, dass ich die vorliegende Arbeit selbstständig verfasst und keine anderen als die angegebenen Quellen und Hilfsmittel benutzt habe. Mit einer Veröffentlichung dieser Arbeit durch die Universität Hamburg erkläre ich mich einverstanden.

(Lars Buntemeyer)
Hamburg, den 21. September 2009